

Long-time predictive modeling of nonlinear dynamical systems using neural networks

Shaowu Pan · Karthik Duraisamy

Received: date / Accepted: date

Abstract We study the use of feedforward neural networks (FNN) to develop models of nonlinear dynamical systems from data. Emphasis is placed on predictions at long times, with limited data availability. Inspired by global stability analysis, and the observation of strong correlation between the local error and the maximum singular value of the Jacobian of the ANN, we introduce Jacobian regularization in the loss function. This regularization suppresses the sensitivity of the prediction to the local error and is shown to improve accuracy and robustness. Comparison between the proposed approach and sparse polynomial regression is presented in numerical examples ranging from simple ODE systems to nonlinear PDE systems including vortex shedding behind a cylinder, and instability-driven buoyant mixing flow. Furthermore, limitations of feedforward neural networks are highlighted, especially when the training data does not include a low dimensional attractor. Strategies of data augmentation are presented as remedies to address these issues to a certain extent.

Keywords data-driven modeling · artificial neural networks · Jacobian regularization · machine learning

1 Introduction

The need to model dynamical behavior from data is pervasive across science and engineering. Applications are found in diverse domains such as in control systems [1], time series modeling [2], and describing the evolution of coherent structures [3]. While data-driven modeling of dynamical systems can be broadly classified as a special case of system identification [4], it is important to note certain distinguishing qualities: the learning process may be performed off-line; physical systems may involve very high dimensions; and the goal may involve the prediction of long-time behaviour from limited training data.

Artificial neural networks (ANN) have attracted considerable attention in recent years in domains such as image recognition in computer vision [5,6] and in control applications [7]. The success of ANNs arises from their ability to effectively learn low-dimensional representations from

Shaowu Pan

Department of Aerospace Engineering, University of Michigan, Ann arbor, MI
E-mail: shawnpan@umich.edu

Karthik Duraisamy

Department of Aerospace Engineering, University of Michigan, Ann arbor, MI
E-mail: kdur@umich.edu

complex data, and in building relationships between features and outputs. Neural networks with a single hidden layer and nonlinear activation function are guaranteed to be able to predict any Borel measurable function to any degree of accuracy on a compact domain [8].

The idea of leveraging neural networks to model dynamical systems has been explored since the 1990s. ANNs are prevalent in the system identification and time series modeling community [9, 10, 11, 12], where the mapping between inputs and outputs is of prime interest. Billings et al. [13] explored connections between neural networks and the nonlinear autoregressive moving average model (NARMAX) with exogenous inputs. It was shown that neural networks with one hidden layer and sigmoid activation function represents an infinite series consisting of polynomials of the input and state units. Elanayar et al. [14] proposed the approximation of nonlinear stochastic dynamical systems using radial basis feedforward neural networks. Early work using neural networks to forecast multivariate time series of commodity prices [15] demonstrated its ability to model stochastic systems without knowledge of the underlying governing equations. Tsung et al. [16] proposed learning the dynamics in phase space using a feedforward neural network with time-delayed coordinates.

Paez and Urbina [17, 18, 19] modeled a nonlinear hardening oscillator using a neural network-based model combined with dimension reduction using canonical variate analysis (CVA). Smaoui [20, 21, 22] pioneered the use of neural networks to predict fluid dynamic systems such as the unstable manifold model for bursting behavior in the 2-D Navier-Stokes and the Kuramoto-Sivashinsky equations. The dimensionality of the original PDE system is reduced by considering a small number of POD (proper orthogonal decomposition) coefficients. Interestingly, similar ideas of using principal component analysis for dimension reduction can be traced back to work in cognitive science by Elman [23]. Elman also showed that knowledge of the intrinsic dimensions of the system can be very helpful in determining the structure of the neural network. However, in the majority of the results [20, 21, 22], the neural network model is only evaluated a few time steps from the training set, which might not be a stringent performance test if longer time predictions are of interest.

ANNs have also been applied to chaotic nonlinear systems that are challenging from a data-driven modeling perspective, especially if long time predictions are desired. Instead of minimizing the pointwise prediction error, Bakker et al. [24] satisfied the Diks' criterion in learning the chaotic attractor. Later, Lin et al. [25] demonstrated that, even the simplest feedforward neural network for nonlinear chaotic hydrodynamics can show consistency in the time-averaged characteristics, power spectra, and Lyapunov exponent between the measurements and the model.

A major difficulty in modeling dynamical systems is the issue of memory. It is known that even for a Markovian system, the corresponding reduced-dimensional system could be non-Markovian [26, 27].

In general, there are two main ways of introducing memory effects in neural networks. First, a simple workaround for feedforward neural networks (FNN) is to introduce time delayed states in the inputs [11]. However, the drawback is that this could potentially lead to an unnecessarily large number of parameters [28]. To mitigate this, Bakker [24] considered following Broomhead and King [29] in reducing the dimension of the delay vector using weighted principal component analysis (PCA). While the second approach uses output or hidden units as additional feedback. As an example, Elman's network [28] is a recurrent neural network (RNN) that incorporates memory in a dynamic fashion.

Miyoshi et al. [30] demonstrated that recurrent RBF networks have the ability to reconstruct simple chaotic dynamics. Sato et al. [31] showed evolutionary algorithms can be used to train recurrent neural networks to capture the Lorenz system. Bailer-Jones et al. [32] used a standard RNN to predict the time derivative in discrete or continuous form for simple dynamical systems; this can be considered an RNN extension to Tsung's phase space learning [16]. Wang et al. [33]

proposed a framework combining POD for dimension reduction and long-short-term memory (LSTM) recurrent neural networks, and applied it to a fluid dynamic system.

We limit ourselves to feedforward neural networks, since there are still many unanswered questions about modeling dynamical systems even in this simplest form. It is known that time delayed FNNs closely resemble simple RNNs trained with teacher forcing [34]. Further, RNNs are not easy to train since standard training algorithms (e.g., back propagation through time [35]) are likely to introduce stronger overfitting than FNN due to vanishing gradients [34]. Recently, sparse regression (SINDy) [3, 36] has gained popularity as a tool for data-driven modeling. The idea is to search for a sparse representation of a linear combination of functions selected from a library. In this work, we will compare it with FNN-based models and highlight some differences.

The paper is organized as follows: the problem description is provided in section 2 and the mathematical formulation of standard and Jacobian-regularized FNNs is presented in section 3. Results and discussion are presented in section 4. We first present a comparison with SINDy for simple dynamical systems. Then we highlight the importance of stabilization to control the global error of predicted trajectory and the impact of Jacobian regularization. Finally, we apply the model in a nonlinear PDE system where a low dimensional attractor is not realized and discuss the limitations of black-box modeling of dynamical system and propose data augmentation as remedies. Conclusions are drawn in section 5.

2 Problem description

Consider dynamics of interest represented by a discrete Markovian system governed by the mapping \mathbf{F} :

$$\mathbf{x}^{n+1} = \mathbf{F}(\mathbf{x}^n), \quad (1)$$

where $\mathbf{x}^0 = \mathbf{x}(t=0)$ is the known initial condition, and $\mathbf{x}^i \in \mathbb{R}^M$ where $i = 0, \dots, N-1$, $M \in \mathbb{N}^+$ is the dimension of the state vector. $\mathbf{F} : \mathbb{R}^M \mapsto \mathbb{R}^M$ is the unknown state transition map. Given a time series of length N of the states as training data, the goal is to find an approximate mapping function $f(\cdot)$ that can reproduce the dynamical system approximately for unseen test data, i.e., to learn a Markovian evolutionary model for the dynamical system from limited training data that will work in unseen testing conditions.

$$\mathbf{x}^{n+1} \approx f(\mathbf{x}^n). \quad (2)$$

Alternatively, if the data is sampled from a continuous dynamical system, it becomes more natural to model the time derivative as follows

$$(\mathbf{x}^{n+1} - \mathbf{x}^n)/\Delta t \approx f(\mathbf{x}^n), \quad \text{or} \quad \dot{\mathbf{x}}^n \approx f(\mathbf{x}^n). \quad (3)$$

Depending on the way one defines the training and testing set, two types of problems are considered in the current work:

1. prediction of a certain trajectory starting from an initial condition that is different from the training trajectories.
2. prediction of the future trajectory given past information of the trajectory as training data.

Conservatively speaking, the success of tackling the first of the above problems requires the trajectories in the training data to be representative of the distribution in the region of interest, which may or may not be feasible depending on how informative the data is. In the context of modeling dynamical systems, it is often implied in previous literature [21] that the initial condition of unseen testing data is not far away from the training data. The second problem can also be difficult since it will challenge the effectiveness of the model as past information might not

be sufficient for the model to be predictive on unseen data. Again, it is often implied in previous works [33, 37, 22], successful predictions are often accompanied by an underlying low dimensional attractor so the past states as training data can be collected until it becomes representative of the future.

3 Mathematical Modeling Framework

In this section, we first define metrics of model performance, then introduce the standard FNN model and the Jacobian-regularized FNN model. Finally, techniques to mitigate overfitting are described.

3.1 Definitions of error metrics

To measure the prediction error for each sample in an *a priori* sense (i.e., given exact \mathbf{x}^i), we define the local error vector $\xi_{local}^i \in \mathbb{R}^M$ for the i -th sample $(\mathbf{x}^i, \mathbf{y}^i)$ by eq. (4)

$$\xi_{local}^i = \mathbf{y}^i - f(\mathbf{x}^i), \quad (4)$$

and define local error at the i -th sample by eq. (5):

$$e_{local}^i = \|\xi_{local}^i\|_2 = \|\mathbf{y}^i - f(\mathbf{x}^i)\|_2, \quad (5)$$

where $\|(\cdot)\|_2 : \mathbb{R}^M \mapsto \mathbb{R}$ is the vector 2-norm and $|\cdot| : \mathbb{R} \mapsto \mathbb{R}$ is the absolute value operator.

We can further define the local error of the i -th sample for the j -th component as shown in eq. (6)

$$e_{local,j}^i = |y_j^i - f(\mathbf{x}^i)_j|. \quad (6)$$

The local error assumes that the i^{th} input feature, \mathbf{x}_i is predicted accurately. On the other hand, the global error vector is defined in eq. (7), in which $\widehat{\mathbf{x}}^i$ is obtained by *iterative prediction*, i.e., *a posteriori evaluation*, at the i -th step from an initial condition through either time integration or transition function as a discrete map. That is $\widehat{\mathbf{x}}^i$ is obtained from $f(\widehat{\mathbf{x}}^{i-1})$ in a recursive sense.

$$\xi_{global}^i = \mathbf{x}^i - \widehat{\mathbf{x}}^i. \quad (7)$$

Similarly, the global error is defined in eq. (8)

$$e_{global}^i = \|\xi_{global}^i\|_2 = \|\mathbf{x}^i - \widehat{\mathbf{x}}^i\|_2, \quad (8)$$

and for the j -th component specifically in eq. (9),

$$e_{global,j}^i = |x_j^i - \widehat{x}_j^i|. \quad (9)$$

Further, to obtain a holistic view for model performance in the feature space, if the ground truth \mathbf{F} is known, we can define stepwise error shown in eq. (10) as the local error at any arbitrary point in the feature space of interest

$$e_{stepwise}(\mathbf{x}) = \|\mathbf{F}(\mathbf{x}) - f(\mathbf{x})\|_2. \quad (10)$$

Note that $e_{stepwise}$ is not restricted by the training or testing trajectory, but is arbitrary in the region of interest.

Finally, R^2 as a standard scalar metric for regression performance is defined as $R^2 = \frac{1}{M} \sum_{j=0}^{M-1} R_j^2$, i.e., the uniform averaged coefficient of determination on the validation data.

$$R_j^2 = R^2(\mathbf{y}_j, \widetilde{\mathbf{y}}_j) = 1 - \frac{\sum_{i=0}^{n_{sample}-1} (y_j^i - \widetilde{y}_j^i)^2}{\sum_{i=0}^{n_{sample}-1} (y_j^i - \bar{y}_j)^2}, \quad (11)$$

where $\bar{y}_j = \frac{1}{n_{sample}} \sum_{i=0}^{n_{sample}-1} y_j^i$ and $\widetilde{\mathbf{y}}^i = f(\mathbf{x}^i)$.

3.2 Feedforward neural network model

3.2.1 Basic model: densely connected feedforward neural network

To approximate the ground truth function \mathbf{F} , our basic model uses an approximation f by a feedforward neural network shown in eq. (3). The existence of an arbitrarily accurate feedforward neural network given enough number of hidden units is guaranteed from the property of the universal approximator [38]. It should be noted that our basic model is related to Tsung's phase-space-learning model [16]. If the Markovian assumption is adopted, the training feature matrix snapshots X and training target matrix snapshots Y are as follows:

$$X = \begin{bmatrix} x_1^0 & x_2^0 & x_3^0 & \dots & x_M^0 \\ x_1^1 & x_2^1 & x_3^1 & \dots & x_M^1 \\ \dots & \dots & \dots & \dots & \dots \\ x_1^{N-1} & x_2^{N-1} & x_3^{N-1} & \dots & x_M^{N-1} \end{bmatrix} \in \mathbb{R}^{N \times M}, \quad (12)$$

and

$$Y = \begin{bmatrix} y_1^0 & y_2^0 & y_3^0 & \dots & y_M^0 \\ y_1^1 & y_2^1 & y_3^1 & \dots & y_M^1 \\ \dots & \dots & \dots & \dots & \dots \\ y_1^{N-1} & y_2^{N-1} & y_3^{N-1} & \dots & y_M^{N-1} \end{bmatrix} \in \mathbb{R}^{N \times M}, \quad (13)$$

where M is the dimension of the state, N is the total number of snapshots of training data, learning target Y is the time derivative, and the subscript stands for the index of the component. Note that each component of the feature and target are normalized to zero mean and unit variance for better training performance in the neural network.

By generally constructing a densely connected feedforward neural network $f(\cdot): \mathbb{R}^M \mapsto \mathbb{R}^M$ with $L - 1$ hidden layers and output layer as linear, the following recursive expression is defined for each hidden layer:

$$\boldsymbol{\eta}^l = \sigma_l(W_l \boldsymbol{\eta}^{l-1} + b_l), \quad l = 1, \dots, L - 1, \quad (14)$$

where $\boldsymbol{\eta}^0$ stands for the input of the neural network \mathbf{x} , $\boldsymbol{\eta}^l \in \mathbb{R}^{n_l}$, $n_l \in \mathbb{N}^+$ is the number of hidden units in layer l , and σ_l is the activation function of layer l .

Note that the output layer is linear, i.e., $\sigma_L(x) = x$:

$$f(\mathbf{x}; \mathbf{W}^L, \mathbf{b}^L) = \boldsymbol{\eta}^L = W_L \boldsymbol{\eta}^{L-1} + b_L, \quad (15)$$

where parameters of the neural network are $\mathbf{W}^L = \{W_i\}_{i=1, \dots, L}$, $\mathbf{b}^L = \{b_i\}_{i=1, \dots, L}$.

For example, if we consider using two hidden layers where $L = 3$ and the number of hidden units are the same, the full expression for the neural network model is given as

$$\mathbf{y} = f(\mathbf{x}; \mathbf{W}, \mathbf{b}) = W_3 \sigma(W_2 \sigma(W_1 \mathbf{x} + b_1) + b_2) + b_3, \quad (16)$$

where $\mathbf{x} \in \mathbb{R}^M$ is the state of the dynamical system and $\mathbf{y} \in \mathbb{R}^M$ is modeling target, i.e., time derivative of the states. $\sigma(\cdot): \mathbb{R} \mapsto \mathbb{R}$ is a nonlinear activation function. $W_1 \in \mathbb{R}^{n_h \times M}$, $W_2 \in \mathbb{R}^{n_h \times n_h}$, $W_3 \in \mathbb{R}^{M \times n_h}$. $b_1 \in \mathbb{R}^{n_h}$, $b_2 \in \mathbb{R}^{n_h}$, $b_3 \in \mathbb{R}^M$. Sets of weights and biases are $\mathbf{W}^3 = \{W_1, W_2, W_3\}$ and $\mathbf{b}^3 = \{b_1, b_2, b_3\}$. The problem of determining the neural network model is equivalent to finding the parameters of a neural network that minimizes the mean-square Euclidean norm between the prediction and target vector in the form

$$\mathbf{W}^*, \mathbf{b}^* = \arg \min_{\mathbf{W}^3, \mathbf{b}^3} \frac{1}{|I_{train}|} \sum_{i \in I_{train}} \|f(\mathbf{x}^i; \mathbf{W}^3, \mathbf{b}^3) - \mathbf{y}^i\|_2^2, \quad (17)$$

where I_{train} is the index set of training data, and \mathbf{x}^i and \mathbf{y}^i correspond to the i -th feature-target pair.

For this high dimensional optimization problem, we follow the standard procedure of initializing weights using a truncated normal distribution to potentially avoid saturation and employing the Adam optimizer [39], which belongs to the family of first-order gradient-based methods. Unfortunately, due to the non-convex nature of eq. (17), for such a high degree of freedom of parameters, one can only afford to find a local minimum instead of the global minimum. In practice, however, a good local minimum is usually satisfactory [34]. Hyperparameters considered in current work for the basic model are the number of units for each hidden layer n_h and activation function $\sigma(\cdot)$, which will be selected heuristically using grid search over a range of feasible configurations. The artificial neural network model is implemented in Python using the Tensorflow library [40].

3.2.2 Jacobian regularized model

In standard FNNs, minimizing mean-squared-error on the training data only guarantees model performance in terms of the local training error. It does not guarantee the stability of the trajectory which is referred here as the possibility of the global error growing unboundedly over the course of a long-term prediction due to accumulation of local error.

Here, we take a closer look at the error propagation in a dynamical system for the FNN model when evaluated in an iterative fashion. Without any loss of generality, assuming the map f that approximates a discrete transition function is given

$$\widehat{\mathbf{x}}^{i+1} = f(\widehat{\mathbf{x}}^i), \quad (18)$$

the relation between the local and global error is given by

$$\xi_{global}^{i+1} = \mathbf{x}^{i+1} - \widehat{\mathbf{x}}^{i+1} = \mathbf{F}(\mathbf{x}^i) - f(\widehat{\mathbf{x}}^i) = \mathbf{F}(\widehat{\mathbf{x}}^i + \xi_{global}^i) - f(\widehat{\mathbf{x}}^i), \quad (19)$$

$$\xi_{global}^{i+1} = \mathbf{F}(\widehat{\mathbf{x}}^i + \xi_{global}^i) - f(\widehat{\mathbf{x}}^i + \xi_{global}^i) + f(\widehat{\mathbf{x}}^i + \xi_{global}^i) - f(\widehat{\mathbf{x}}^i). \quad (20)$$

Consider a Taylor expansion of $f(\widehat{\mathbf{x}}^i + \xi_{global}^i)$ about $\widehat{\mathbf{x}}^i$, we have

$$\xi_{global}^{i+1} = \mathbf{F}(\widehat{\mathbf{x}}^i + \xi_{global}^i) - f(\widehat{\mathbf{x}}^i + \xi_{global}^i) + \left. \frac{\partial f}{\partial \mathbf{x}} \right|_{\mathbf{x}=\widehat{\mathbf{x}}^i} \xi_{global}^i + \frac{1}{2} \xi_{global}^i{}^T H \xi_{global}^i + \dots, \quad (21)$$

where H is the Hessian matrix evaluated at some point between $\widehat{\mathbf{x}}^i$ and $\widehat{\mathbf{x}}^i + \xi_{global}^i$.

Assuming $\|\xi_{global}^i\|_2 \ll 1$, $\|H\|_2$ is bounded, and the Hessian term is negligible compared to the Jacobian term we have

$$e_{global}^{i+1} \leq e_{local}^i + \left\| \left. \frac{\partial f}{\partial \mathbf{x}} \right|_{\mathbf{x}=\widehat{\mathbf{x}}^i} \right\|_2 e_{global}^i + o(e_{global}^i) \leq e_{local}^i + \left\| \left. \frac{\partial f}{\partial \mathbf{x}} \right|_{\mathbf{x}=\widehat{\mathbf{x}}^i} \right\|_F e_{global}^i + o(e_{global}^i). \quad (22)$$

Similarly, in a continuous setting, if target is the time derivative, we have

$$e_{global}^{i+1} \leq e_{global}^i + \int_{i\Delta t}^{(i+1)\Delta t} e_{local}^{\tau/\Delta t} d\tau + \int_{i\Delta t}^{(i+1)\Delta t} \left\| \left. \frac{\partial f}{\partial \mathbf{x}} \right|_{\mathbf{x}=\widehat{\mathbf{x}}^i} \right\|_F e_{global}^{\tau/\Delta t} d\tau + o(e_{global}^i \Delta t), \quad (23)$$

$$e_{global}^{i+1} \leq \left(1 + \Delta t \left\| \left. \frac{\partial f}{\partial \mathbf{x}} \right|_{\mathbf{x}=\widehat{\mathbf{x}}^i} \right\|_F \right) e_{global}^i + \int_{i\Delta t}^{(i+1)\Delta t} e_{local}^{\tau/\Delta t} d\tau + o(e_{global}^i \Delta t). \quad (24)$$

The right hand sides of eq. (22) and eq. (24) contain contributions from the global error and accumulation of local error. Optimization as in eq. (17) can minimize the latter term, but not

necessarily the former. This suggests that manipulating the eigenspectrum of the Jacobian might be beneficial for stabilization by suppressing the growth of the error. Due to the simplicity of computing the Frobenius norm compared to the 2-norm, we consider penalizing the Frobenius norm of the Jacobian of the neural network model. In the context of improving generalization performance of input-output neural network models, similar regularization has been also proposed by Rifai [41]. It should be noted that our purpose is to achieve better error dynamics in a temporal sense, which differs from the generalization goal in deep learning. Thus, one may seek a locally optimal solution that can suppresses the growth in global error while minimizing the local error.

The regularized loss function inspired from the above discussion is thus

$$\mathbf{W}^*, \mathbf{b}^* = \arg \min_{\mathbf{W}, \mathbf{b}} \frac{1}{N_{train}} \sum_{i \in I_{train}} \|f(\mathbf{x}^i; \mathbf{W}, \mathbf{b}) - \mathbf{y}^i\|_2^2 + \lambda \|J(\mathbf{x}^i; \mathbf{W}, \mathbf{b})\|_F^2, \quad (25)$$

where J is the Jacobian of the neural network output with respect to the input, and λ is a hyperparameter. On one hand, it should be noted that regularizing the Frobenius norm of the eigenspectrum of the Jacobian indirectly suppresses the magnitude of the eigenvalue of the Jacobian. On the other hand, excessive weighting on the magnitude of the eigenvalue would lead to less weighting on local error, which might result in an undesirably large local error. Thus, λ should be set as a relatively small value without strongly impacting the model performance in an a priori sense.

3.3 Reducing overfitting

Overfitting is a common issue in the training of machine learning models, and it arises when models tend to memorize the training data instead of generalizing true functional relations. In neural networks, overfitting can occur from poor local minima and is partially due to the unavoidable non-convexity of an artificial neural network. Overfitting cannot be completely eliminated for most problems, given the NP-hard nature of the problem. Generally, overfitting can be controlled by three kinds of regularization techniques: The first follows the Occam’s razor principle, e.g., L1 sparsity regularization [3]. However there is no guarantee that Occam’s razor is appropriate for all cases, and finding the optimal sparsity level is often iterative. The second is to smooth the function, e.g., using weight decay [34]. The third type is especially suitable in iterative learning, e.g., early stopping, which is a widely used strategy in the deep learning community [34]. In this work, we found validation-based early stopping to be sufficient. We split the data further into pure training and validation sets, and then monitor overfitting by measuring R^2 .

4 Results & Discussion

Given sequential training data, the capability of the basic FNN is first evaluated in two-dimensional dynamical systems with polynomial non-linearities in section 4.1 and non-polynomial-non-rational dynamics in section 4.2. The basic model is compared with SINDy [3], a method that directly aims to learn functional models using L_1 sparse regression on a dictionary of candidate basis functions. In section 4.3, we demonstrate that the basic model performs better than SINDy on the problem of incompressible flow behind a cylinder, in spite of the explicit addition of quadratic terms to the dictionary. In addition, the local error is found to be strongly correlated with the maximum singular value of the Jacobian, thus serving as an inspiration for Jacobian regularization. In section 4.4, we demonstrate the stabilizing aspect of Jacobian regularization for the problem of laminar wake behind a cylinder, where the system exhibits a low dimensional attractor. In section 4.5, we assess the ability of our regularized FNN model to approximate a

dynamically evolving high-dimensional buoyancy-driven mixing flow system that is characteristic of flow physics driven by instabilities. The results show that, for systems that do not exhibit a low dimensional attractor, it is difficult for a black-box model to have satisfactory long-time prediction capabilities. In section 4.6 we show that predictive properties can be improved by data augmentation in the state space of interest.

4.1 2D polynomial system: Van der Pol oscillator

The first order forward discretized scheme of the Van der Pol (VDP) system is given as

$$\begin{pmatrix} x_1^{n+1} \\ x_2^{n+1} \end{pmatrix} = \begin{pmatrix} x_1^n \\ x_2^n \end{pmatrix} + \Delta t \begin{pmatrix} x_2^n \\ (\mu(1 - x_1^n x_1^n)x_2^n - x_1^n) \end{pmatrix}, \quad (26)$$

where $\Delta t = 0.1$ and $\mu = 2.0$. The modeling target is thus eq. (27)

$$\mathbf{y}^n = \begin{pmatrix} \frac{x_1^{n+1} - x_1^n}{\Delta t} \\ \frac{x_2^{n+1} - x_2^n}{\Delta t} \end{pmatrix} = \begin{pmatrix} x_2^n \\ (\mu(1 - x_1^n x_1^n)x_2^n - x_1^n) \end{pmatrix} = \mathbf{F}(\mathbf{x}^n). \quad (27)$$

Our goal is to reproduce the dynamics governed by \mathbf{F} based on data snapshots. The data distribution of the training and testing features is shown in fig. 1. Note that a few test points demand extrapolation.

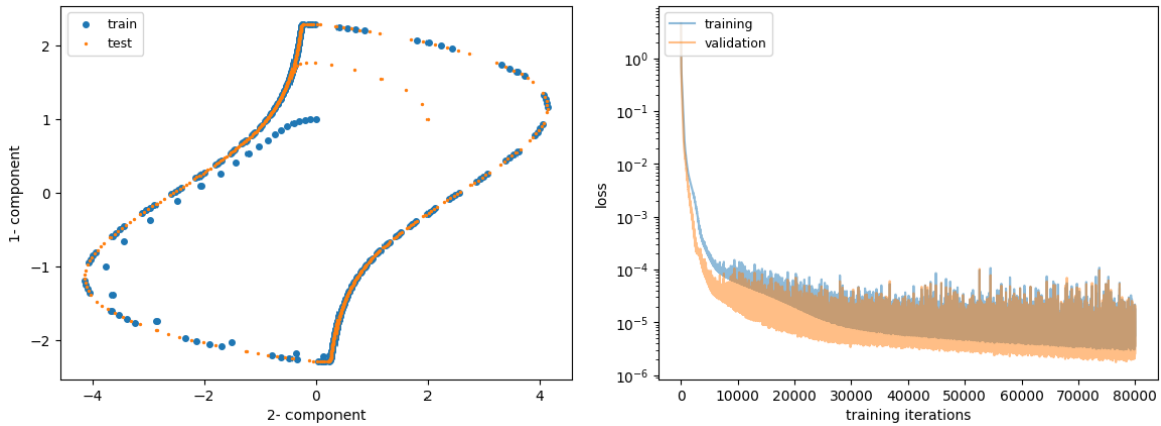


Fig. 1 VDP case. Left: Distribution of training/testing sets. Right: learning rate

The basic model in eq. (17) is optimized using training data from a single trajectory, containing 399 data points. Test data containing 599 points is generated using a different initial condition. Our configuration of hyperparameters is shown in table 1 below. Data is normalized to zero mean and unit standard deviation. We use minibatch training with 64 batches and 80000 epochs to ensure our model arrives at a local minimum of eq. (17). The basic model consists of two

Table 1 Hyperparameter configuration of the basic model: VDP case

layer structure	activation function	loss function	optimizer	learning rate
2-8-8-2	Swish	MSE	Adam	0.002

hidden layers with each layer containing 8 hidden units. Two hidden layers are accompanied by Swish nonlinear activation as $f(x) = x \cdot \text{sigmoid}(\beta x)$ where in practice β is fixed as unity [42]. The output layer is linear. 20% of training data is used as a validation set and we monitor the performance on the validation set as a warning of overfitting. In fig. 1, the learning curve suggests that overfitting is a factor.

As shown in fig. 2, the basic model predicts the \mathbf{F} at each training point very well a priori, but slight phase lag is observed a posteriori in testing, which originates from the initial steps.

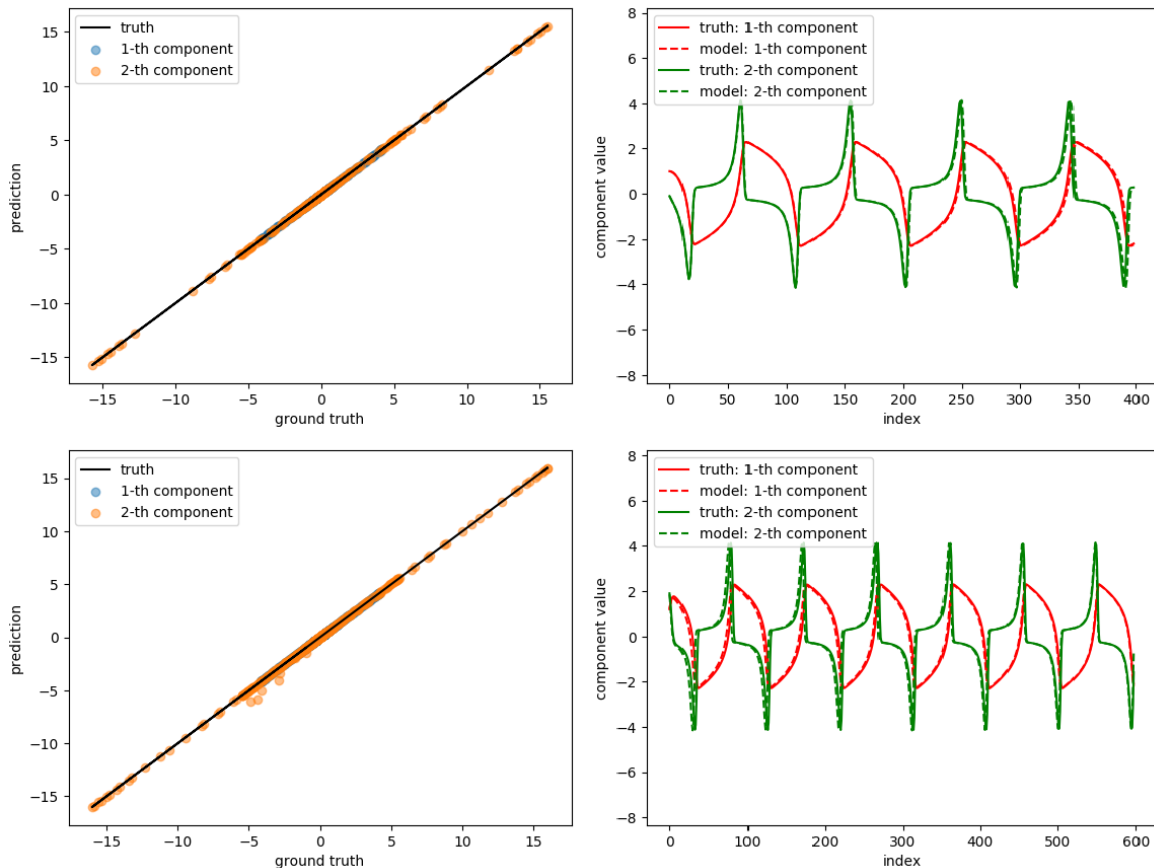


Fig. 2 A priori and a posteriori result of basic model on VDP case: first component. Top: training data. Bottom: testing data. Left: a priori. Right: a posteriori.

The variation of the local and global error together with the maximum singular value of the Jacobian is shown in fig. 3. For training data, e_{local} is observed to be relatively uniform, as expected since the objective optimized is MSE uniformly across all training data points. For testing data, e_{local} exhibits peak values near the beginning of the trajectory as expected, since the first few points are far away from the training data shown in fig. 1. Moreover, it is interesting to observe that in fig. 3, the peak of the temporal history of local/global error shows strong correlation with the maximum singular value of the Jacobian.

As seen in fig. 4, the region of large error close to red (implying the difference of the step-wise vector between neural network prediction and ground truth is large) is located near the corner of figure, where there is a dearth of training points. The model performs well near the training

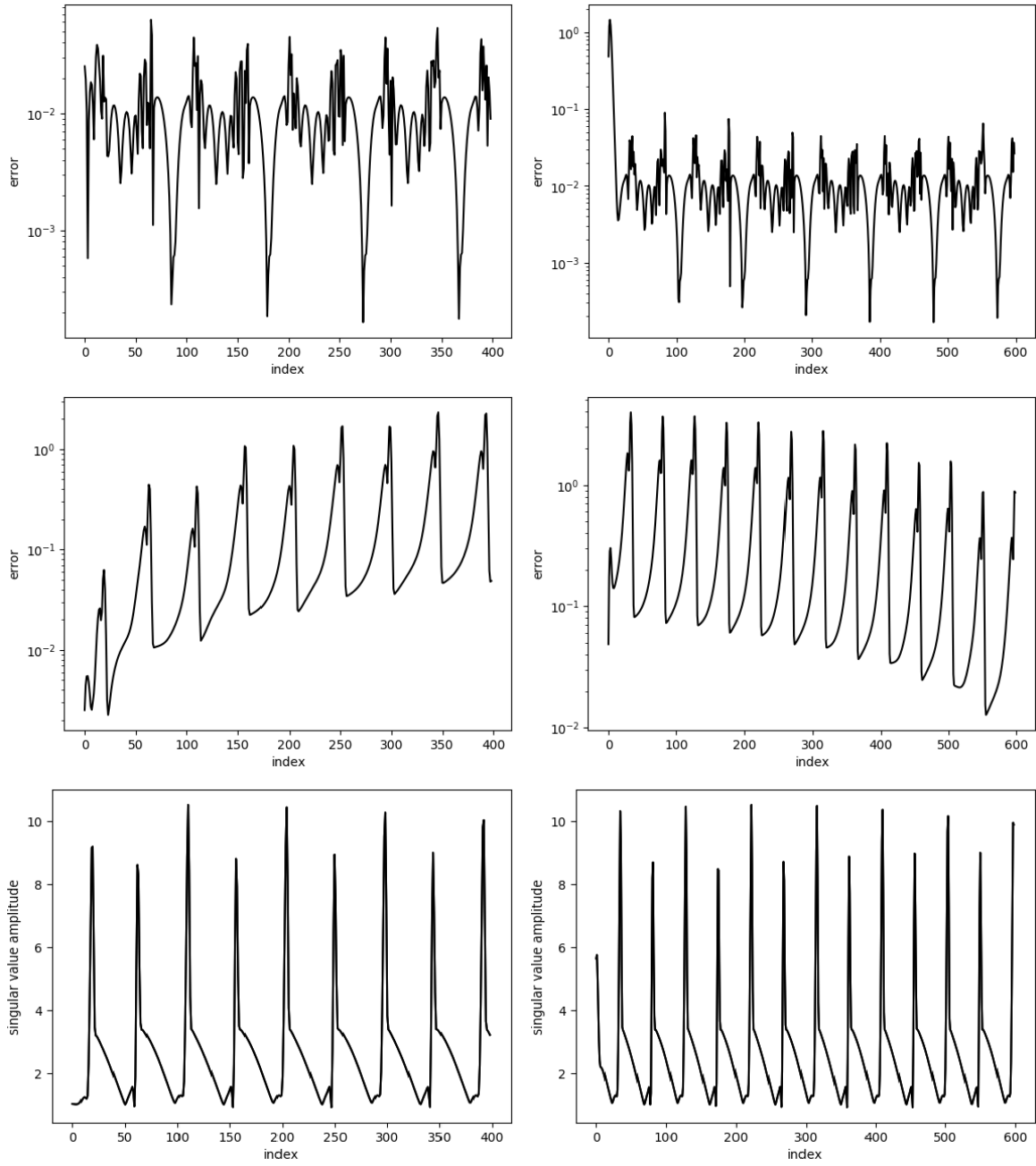


Fig. 3 Variation of local error and global error: basic model on VDP case. Red: first component. Green: second component. Top: local error. Middle: global error. Bottom: maximum singular value of Jacobian evaluated in a local sense. Left: training data. Right: testing data.

points as expected. In this case, since testing data is not very far away from the training data, a good performance can be expected.

For comparison, results obtained from SINDy [3] are shown below in fig. 5, with threshold parameter 2×10^{-4} , maximum polynomial order 3, and no validation data set considered. It should be noted that the excellent result of SINDy shows the advantage of finding the global

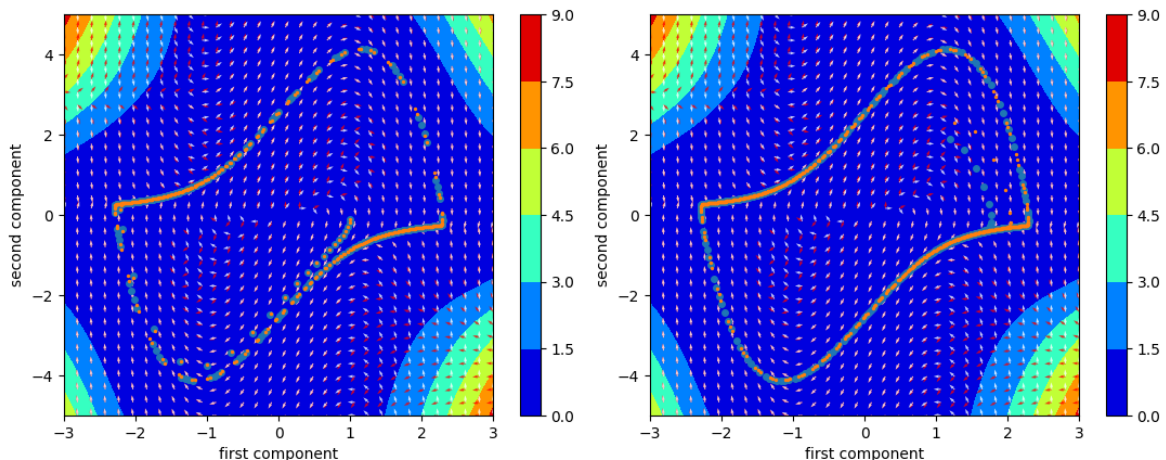


Fig. 4 Stepwise error contour of basic model on VDP case. Left: training data. Right: testing data. Blue dot: ground truth. Orange dot: prediction. White arrow: direction of target vector of ground truth. Red arrow: direction of target vector of prediction.

features where parameters obtained are not restricted to the scope of training data since the ground truth is governed by sparse polynomials.

4.2 2D non-polynomial system: a non-rational non-polynomial oscillator

The success of SINDy is a consequence of the fact that the underlying system can be represented as a sparse vector in a predefined basis library such as that consisting of polynomial or rational functions [36]. Here, we choose a different case: a non-rational, non-polynomial oscillator with $\Delta t = 0.004$:

$$\begin{pmatrix} x_1^{n+1} \\ x_2^{n+1} \end{pmatrix} = \begin{pmatrix} x_1^n \\ x_2^n \end{pmatrix} + \Delta t \begin{pmatrix} 2.5 - 100 \frac{x_1^n x_2^n}{1 + (x_2^n/0.52)^4} \\ -200 \frac{x_1^n x_2^n}{1 + (x_2^n/0.52)^4} + 9.2 - 2.3x_2^n - 1.28|x_2^n|^{3/2} \end{pmatrix}.$$

Here the basic model eq. (17) is optimized using 1199 data points of a single trajectory. Testing data contains 1799 points. A random 20% of training data is taken as the validation set, but also included in later evaluation. The feature distribution in phase space is shown in fig. 7.

Hyperparameters are listed in table 2 and 128 minibatches and 20000 epochs are used. The training error and validation error is shown in fig. 7.

Table 2 Hyperparameter configuration of basic model: non-rational non-polynomial case

layer structure	activation function	loss function	optimizer	learning rate
2-8-8-2	elu	MSE	Adam	0.005

Results for a priori and a posteriori performance on training and testing data are shown below in fig. 8. The training trajectory is perfectly reconstructed while the predictions show slight deviation.

The distribution of the local and global error is shown in fig. 9. Again, we observe that maximum local/global error correlates with the peaks of the maximum singular value of the

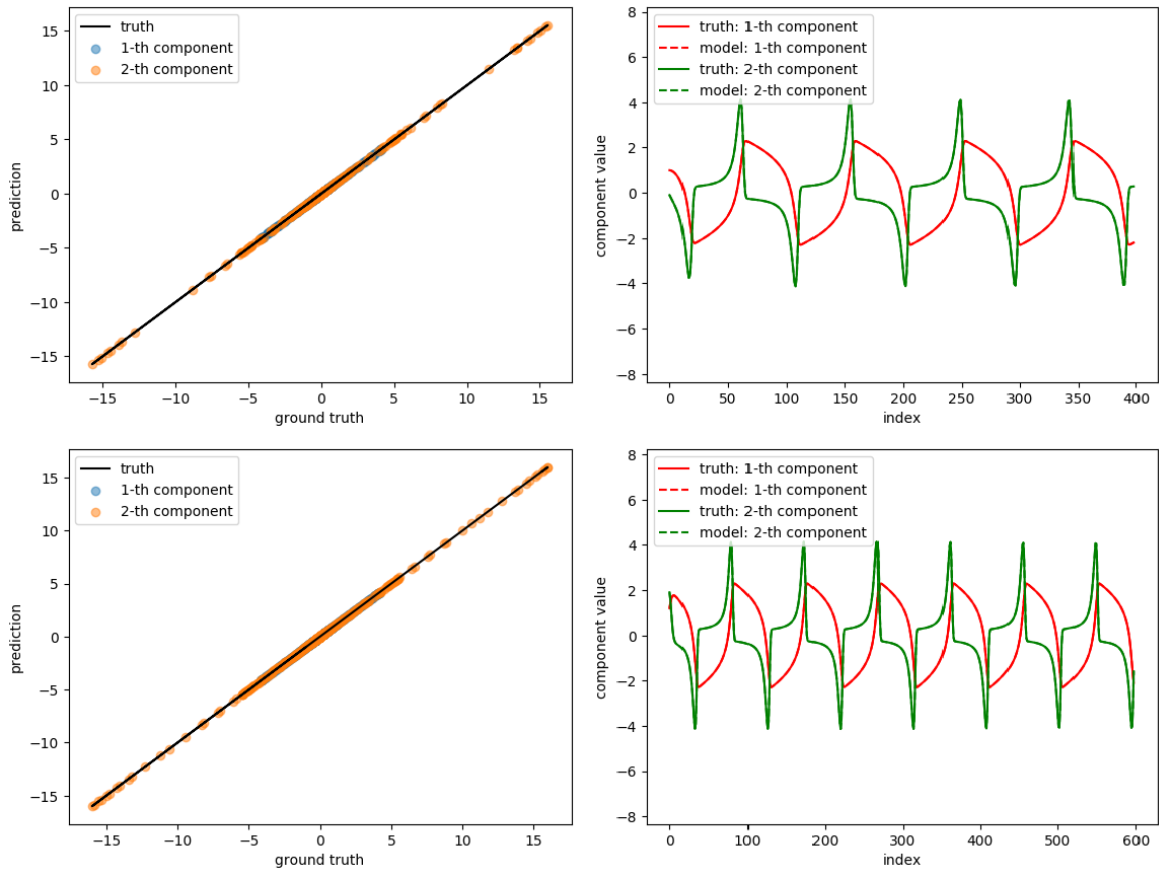


Fig. 5 A priori and a posteriori result of SINDy on VDP case. Top: training data. Bottom: testing data. Left: a priori. Right: a posteriori.

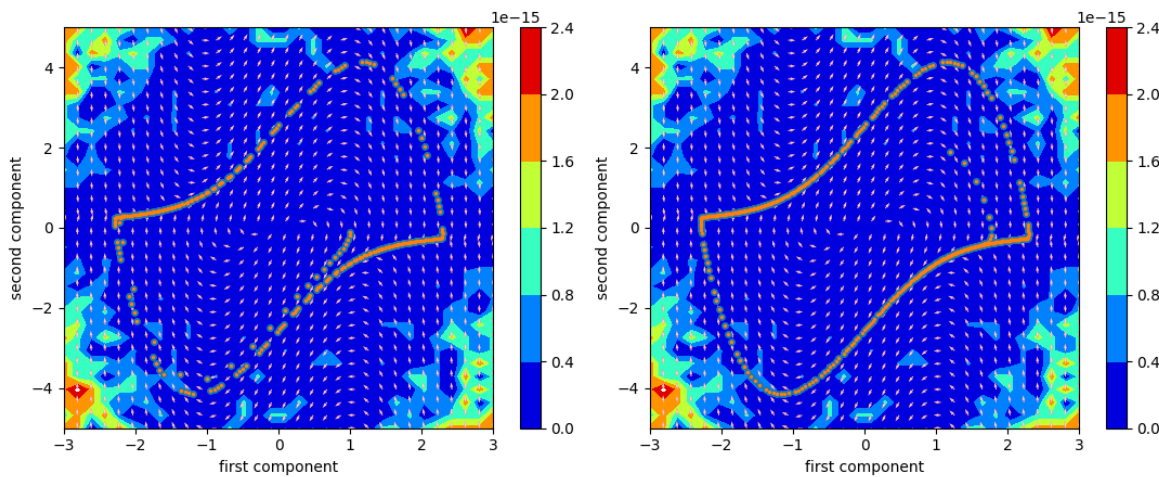


Fig. 6 Stepwise error contour of SINDy on VDP case. Left: training data. Right: testing data. Blue dot: ground truth. Orange dot: prediction. White arrow: direction of target vector of ground truth. Red arrow: direction of target vector of prediction.

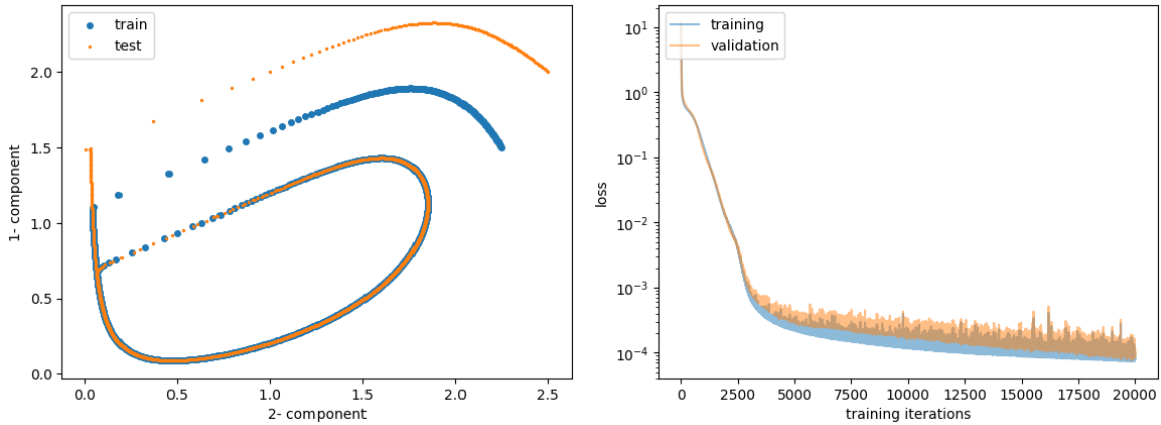


Fig. 7 Non-rational non-polynomial case. Left: data distribution of training/testing feature. Right: learning curve.

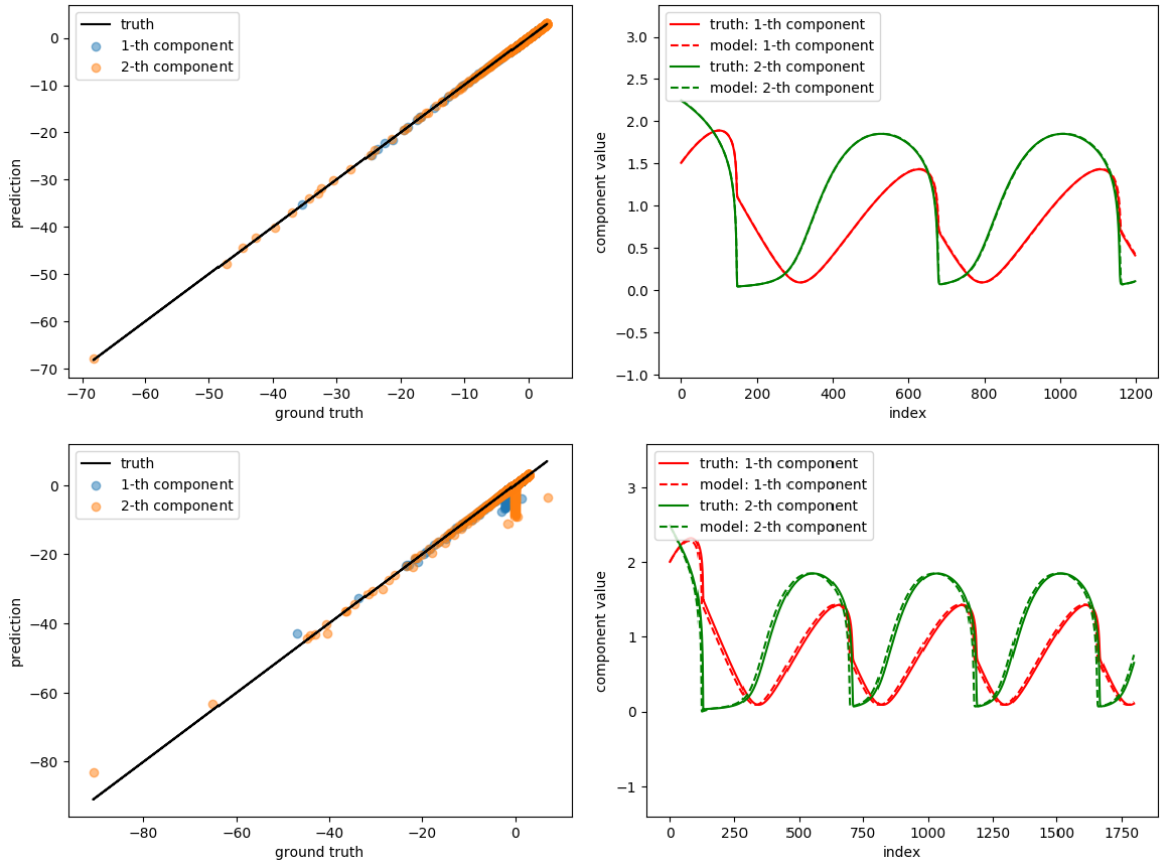


Fig. 8 A priori and a posteriori result of basic model on non-rational non-polynomial case: first component. Top: training data. Bottom: testing data. Left: a priori. Right: a posteriori.

Jacobian. It is interesting to note that the highest local testing error occurs at the peak of the maximum singular value of the Jacobian, instead of at points close to the initial condition.

The error contour in fig. 10 shows that stepwise error around training trajectory is below 0.1. It is important to note that model performance deteriorates at places far away from the training trajectory, especially at the right corner shown in fig. 10.

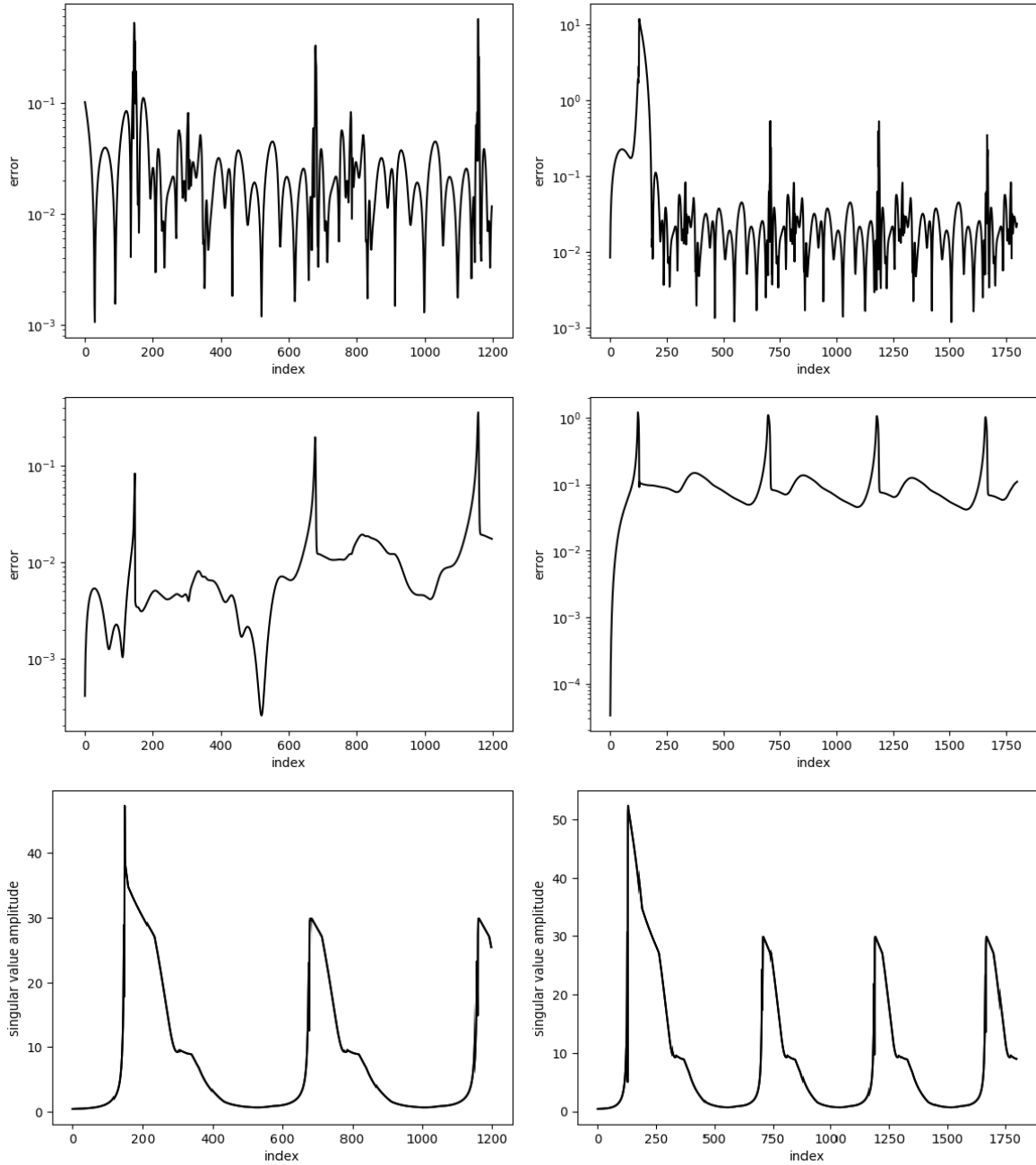


Fig. 9 Variation of local error and global error: basic model on non-rational, non-polynomial case. Red: first component. Green: second component. Top: local error. Middle: global error. Bottom: maximum singular value of Jacobian evaluated in a local sense. Left: training data. Right: testing data.

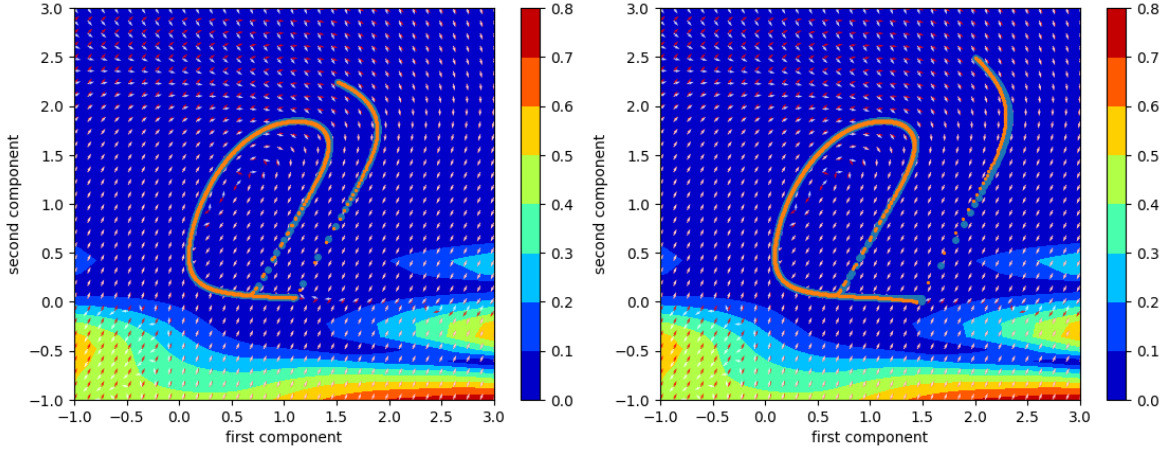


Fig. 10 Stepwise error contour of basic model on non-rational, non-polynomial case. Left: training data. Right: testing data. Blue dot: ground truth. Orange dot: prediction. White arrow: direction of target vector of ground truth. Red arrow: direction of target vector of prediction.

For SINDy, the polynomial order is set to three and threshold as 2×10^{-4} . A priori and a posteriori validation for training and testing is shown in fig. 11. Because there is no sparsity in polynomial basis in this case, it is expected that SINDy cannot reconstruct the dynamics correctly and would perform worse than the basic model.

4.3 Nonlinear PDE system: flow behind a cylinder

In this section, we compare the basic model with SINDy on the problem examined in the original work for SINDy[3]: reconstructing the flow in a cylinder wake. Testing data is generated as a temporal extension of states that lie on a limit cycle at the boundary of training data, which indicates this is not an extrapolation task. For such a high-dimensional nonlinear PDE system, we use two POD modes and one shift mode to reduce the spatial dimension. Training and testing data is the same as in the original work [3] where the first 2999 snapshots in time are used for training, and a later 2994 snapshots used for testing. A random 10% of training snapshots is considered as validation set but also included in later evaluation. The distribution of training data and testing data is shown in fig. 13.

Hyperparameters of the basic model are shown in table 3 with 40000 epochs. For SINDy, the hyperparameters are the same as in previous work [3]. As shown in Figure 14, for training data, SINDy reconstructs a smaller growth rate of oscillating behavior while the basic model accurately reconstructs both the shift mode and two POD modes. For testing data, SINDy contains an observable phase lag for the time period concerned, while the basic model achieves an almost perfect match. This implies that the model obtained from SINDy, although easy to interpret, is not the best model for this dynamical system in terms of accuracy.

Table 3 Hyperparameter configuration of basic model: flow in cylinder wake.

layer structure	activation function	loss function	optimizer	learning rate
2-20-20-2	elu	MSE	Adam	0.001

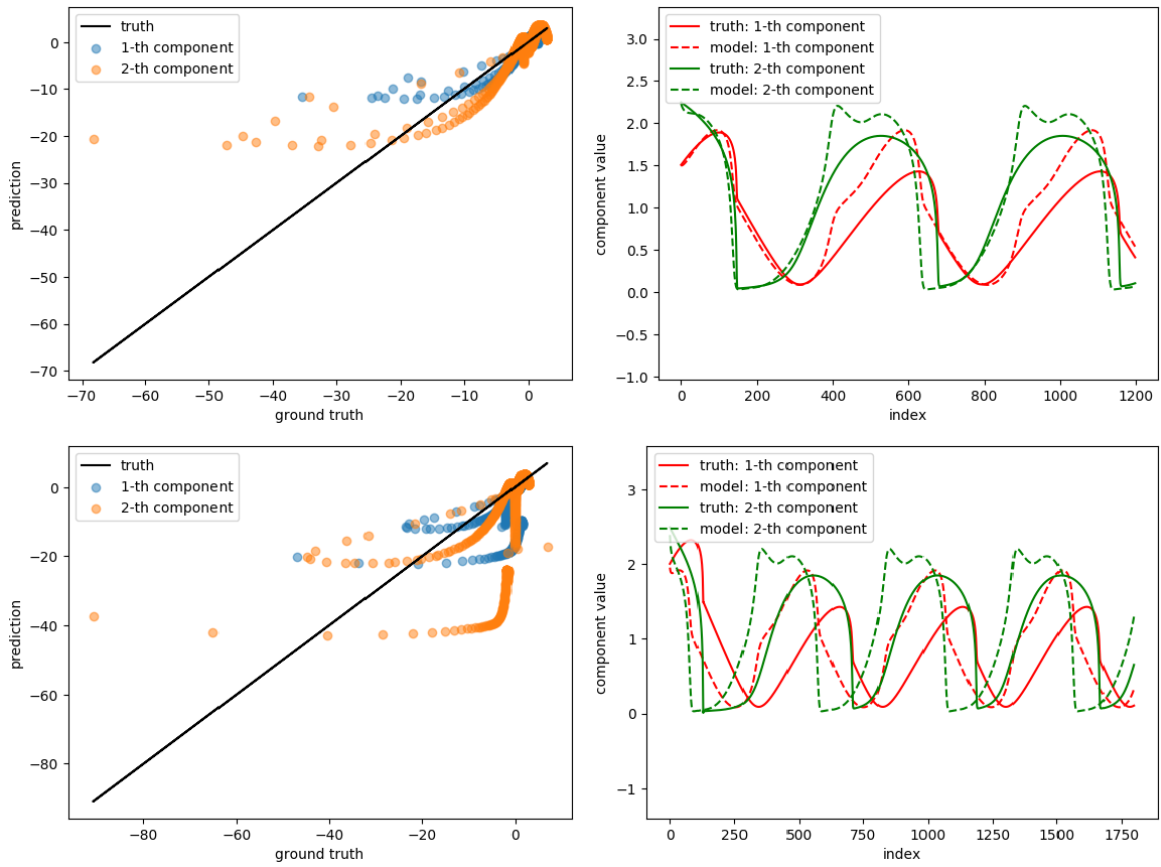


Fig. 11 A priori and a posteriori result of SINDy on non-rational non-polynomial case: first component. Top: training data. Bottom: testing data. Left: a priori. Right: a posteriori.

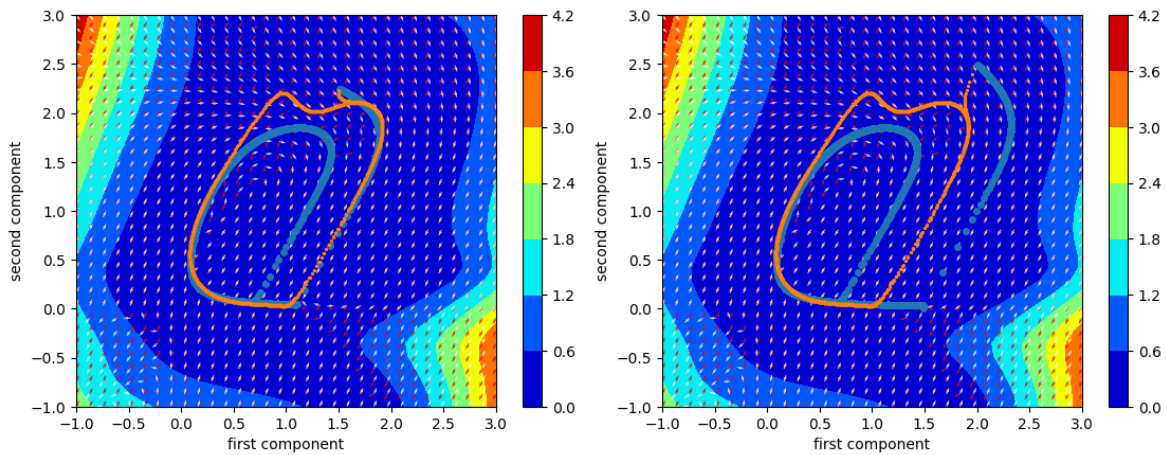


Fig. 12 Stepwise error contour of SINDy on non-rational, non-polynomial case. Left: training data. Right: testing data. Blue dot: ground truth. Orange dot: prediction. White arrow: direction of target vector of ground truth. Red arrow: direction of target vector of prediction.

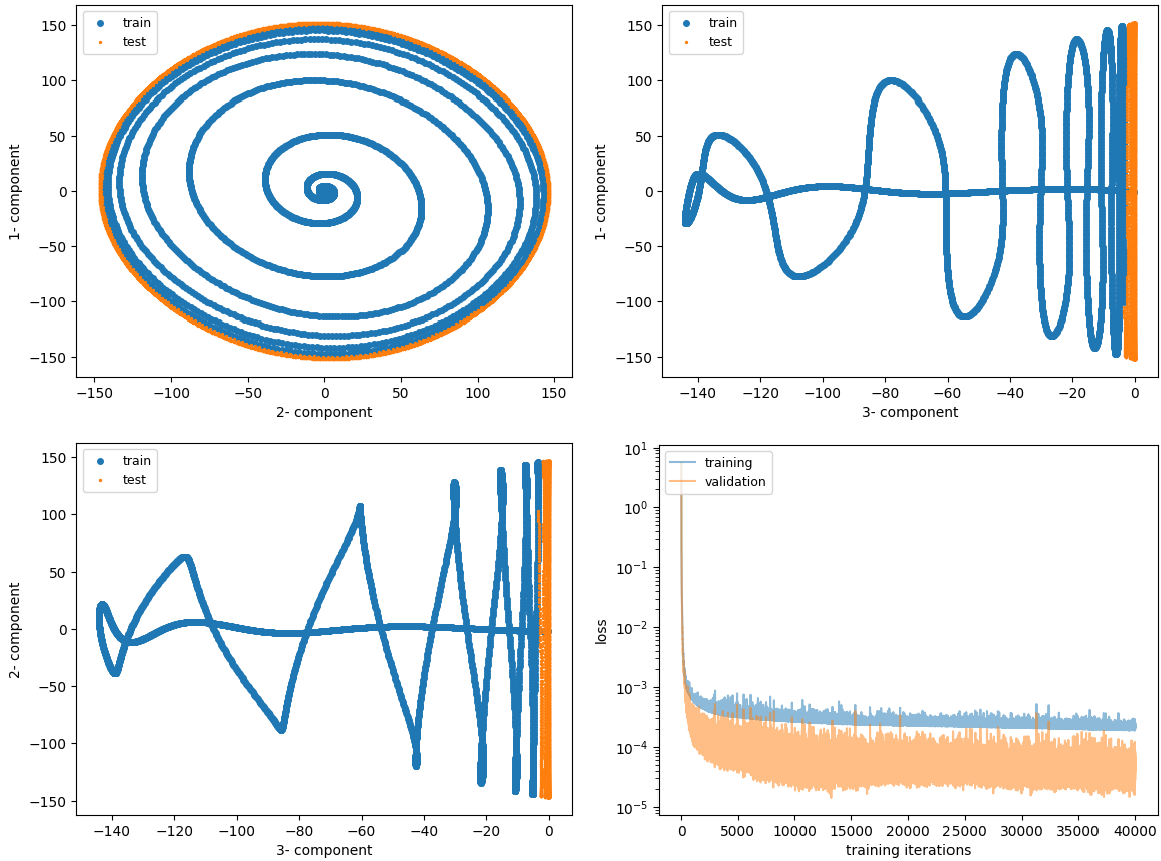


Fig. 13 Flow in cylinder wake. Top left: data distribution of x_1 vs x_2 . Top Right: data distribution of x_1 and x_3 . Bottom left: data distribution of x_2 and x_3 . Bottom right: learning curve.

4.4 Stabilizing the neural network with Jacobian regularization

Due to the non-convexity of the optimization problem that arises in the solution of the basic model in eq. (17), employing a stochastic gradient-descent type method might lead to a solution corresponding to a local minimum, which is often undesirable and difficult to avoid. Most works in the field of deep learning for feedforward neural networks focus on decreasing the impact of poor local minima to promote generalizability. However, in the context of modeling a dynamical system, as it is often assumed that the trajectory of interest is stable with respect to small disturbances [24], the model should be able to approximately reconstruct the training trajectory in the presence of local errors that arise at each step. This would require regularizing instabilities that could arise in a posteriori prediction. To have meaningful comparisons, random number seeds are fixed for initialization of weights and training data shuffling. Nevertheless, we observe that in some cases, for example in the previous case of the cylinder wake, an inappropriate choice of neural network configuration of the basic model, e.g. number of hidden units and type of activation function, can potentially lead to instability in a posteriori evaluation. Such instabilities may materialize even while reconstructing the training trajectory, while the corresponding a priori prediction is almost perfect. Previous work [16] explicitly ensured stability by simply adding more trajectories. Here, we take a different approach by adding a penalty regularization term in the cost function.

In our numerical experiments, with a certain fixed random seed, it is observed that, when the layer structure is 2-20-20-2 with *tanh* as activation function instead of *elu*, the basic model

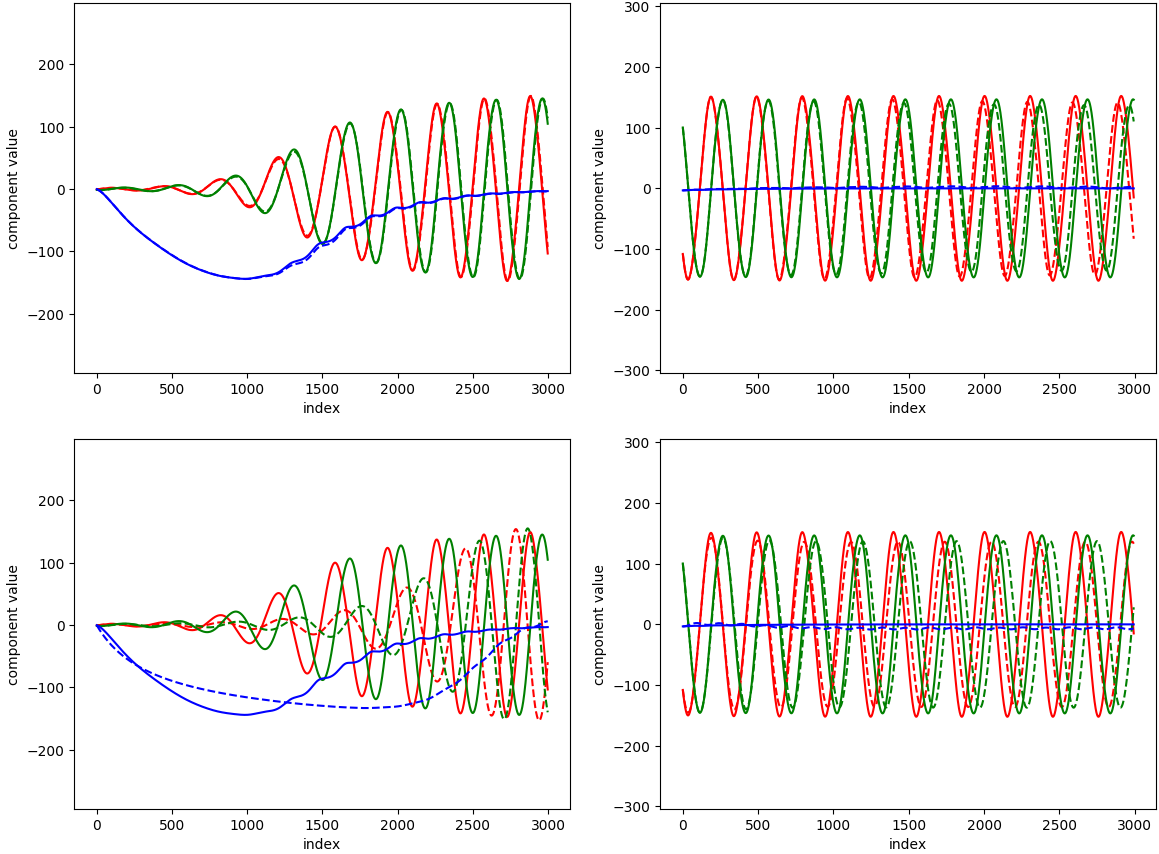


Fig. 14 Flow in cylinder wake. A posteriori comparison between basic model and SINDy. Red: first component. Green: second component. Blue: third component. Top: basic model. Bottom: SINDy. Left: training data. Right: testing data.

becomes numerically unstable after 2000 steps for training data which is displayed in fig. 15. Similar numerical instability is also observed in testing evaluations. However, for the same fixed random seed, the regularized model with $\lambda = 5 \times 10^{-5}$ shows numerically stable results with the same neural network configuration for both training and testing data.

The effectiveness of Jacobian regularization may be attributed to finding a balance between lowering the prediction error, i.e., MSE, and suppressing the sensitivity of the prediction of the future state to the current local error. As shown in fig. 16 and fig. 17, on average, the maximum eigenvalue of the Jacobian is smaller for the regularized model than for the basic model.

Furthermore, the distribution of the eigenvalues of the Jacobian is shown in fig. 18 in the form of a linear stability diagram with explicit 5th order Runge-Kutta time integration. It is clear that the model with Jacobian regularization has significantly smaller positive real eigenvalues. Note that, due to the Frobenius norm, negative real eigenvalues are also decreased in magnitude.

4.5 Nonlinear PDE system: instability-driven buoyant mixing flow

Thus far, we have focused on assessing the performance of the basic and Jacobian-regularized models on nonlinear dynamical systems that either evolve on or towards an attractor. Such systems, even if high-dimensional, can be more easily projected onto a lower dimensional subspace, using for instance, POD. In this section, we consider the Boussinesq buoyant mixing flow [43,

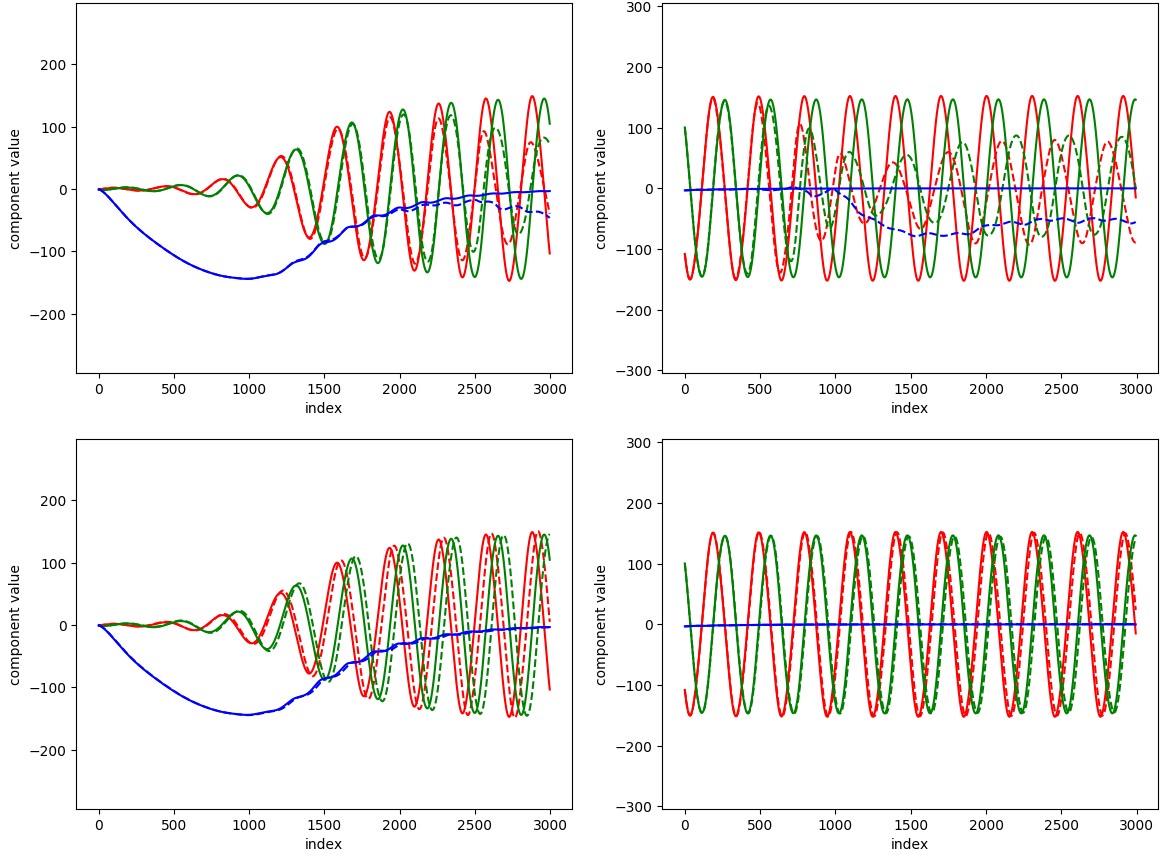


Fig. 15 A posteriori comparison between basic and regularized models for cylinder wake: 3 modes. Red: first component. Green second component. Blue: third component. Top: basic model. Bottom: regularized model. Left: training data. Right: testing data.

44], also known as the unsteady lock-exchange problem [45] which exhibits strong shear and Kelvin-Helmholtz instability phenomena driven by the temperature gradient. Compared to the cylinder flow that evolves on a low-dimensional attractor approaching a limit cycle, the Boussinesq flow is highly convective and instability driven. Consequently, such a system state cannot be represented by a compact set of POD modes. Rather, the low-dimensional manifold itself evolves with time. Further, any noise in the initial data can produce unexpected deviations that makes such systems challenging to model, even using equation-driven reduced order models such as POD-Galerkin [45].

The data set is generated by solving the dimensionless form of the two-dimensional incompressible Boussinesq equations [45], as shown in eq. (28) on a rectangular domain that is $0 < x < 8$ and $0 < y < 1$.

$$\frac{\partial u}{\partial x} + \frac{\partial u}{\partial y} = 0, \quad (28a)$$

$$\frac{\partial u}{\partial t} + u \frac{\partial u}{\partial x} + v \frac{\partial u}{\partial y} = -\frac{\partial P}{\partial x} + \frac{1}{Re} \nabla^2 u, \quad (28b)$$

$$\frac{\partial v}{\partial t} + u \frac{\partial v}{\partial x} + v \frac{\partial v}{\partial y} = -\frac{\partial P}{\partial y} + \frac{1}{Re} \nabla^2 v + Ri\theta, \quad (28c)$$

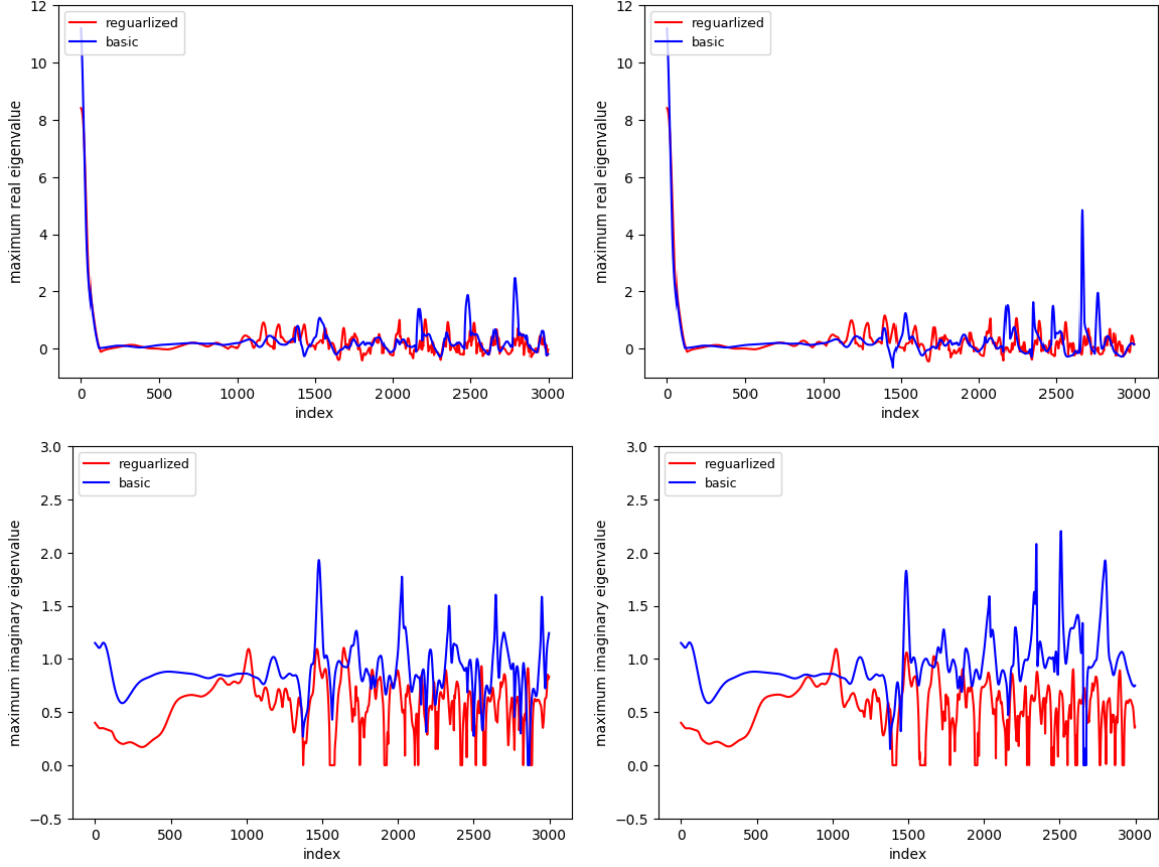


Fig. 16 Flow in cylinder wake. Comparison of eigenvalue of Jacobian between regularized and basic model on training data. Top: maximum real eigenvalue. Bottom: maximum imaginary eigenvalue. Left: a priori. Right: a posteriori.

$$\frac{\partial \theta}{\partial t} + u \frac{\partial \theta}{\partial x} + v \frac{\partial \theta}{\partial y} = \frac{1}{RePr} \nabla^2 \theta, \quad (28d)$$

where u , v , and θ are the horizontal, vertical velocity, and temperature components, respectively. The dimensionless parameters Re , Ri , and Pr are the Reynolds number, Richardson number, and Prandtl number, respectively with values chosen as follows: $Re = 1000$, $Ri = 4.0$, and $Pr = 1.0$. These equations are discretized on a 256×33 grid. Initially, fluids at two different temperatures are separated by a vertical line at $x = 4$. The bounding walls are adiabatic and introduce friction. To obtain an accurate data representation, a fourth-order compact finite difference scheme is used to compute the derivatives in eq. (28). The evolution of the thermal field over the simulation time interval of 32 seconds is shown in fig. 19 and illustrates the highly transient nature of the dynamics. To reduce the dimensionality of the system, POD modes are extracted from the entire data set consisting of 1600 snapshots. The reduced feature set consisting of ten POD weights captures nearly 97% of the total energy is used to train the model and predict the trajectory.

For the setup of training and testing, future state prediction is pursued with the first 70% states of the trajectory treated as training data and the rest for testing. For such a system in 10 dimensions, it is observed that the problem of the a posteriori instability in the basic model becomes more pronounced and difficult to avoid. Challenges of numerical instability were observed even for reconstruction for a wide range of network configurations, and thus results from the basic model are not reported.

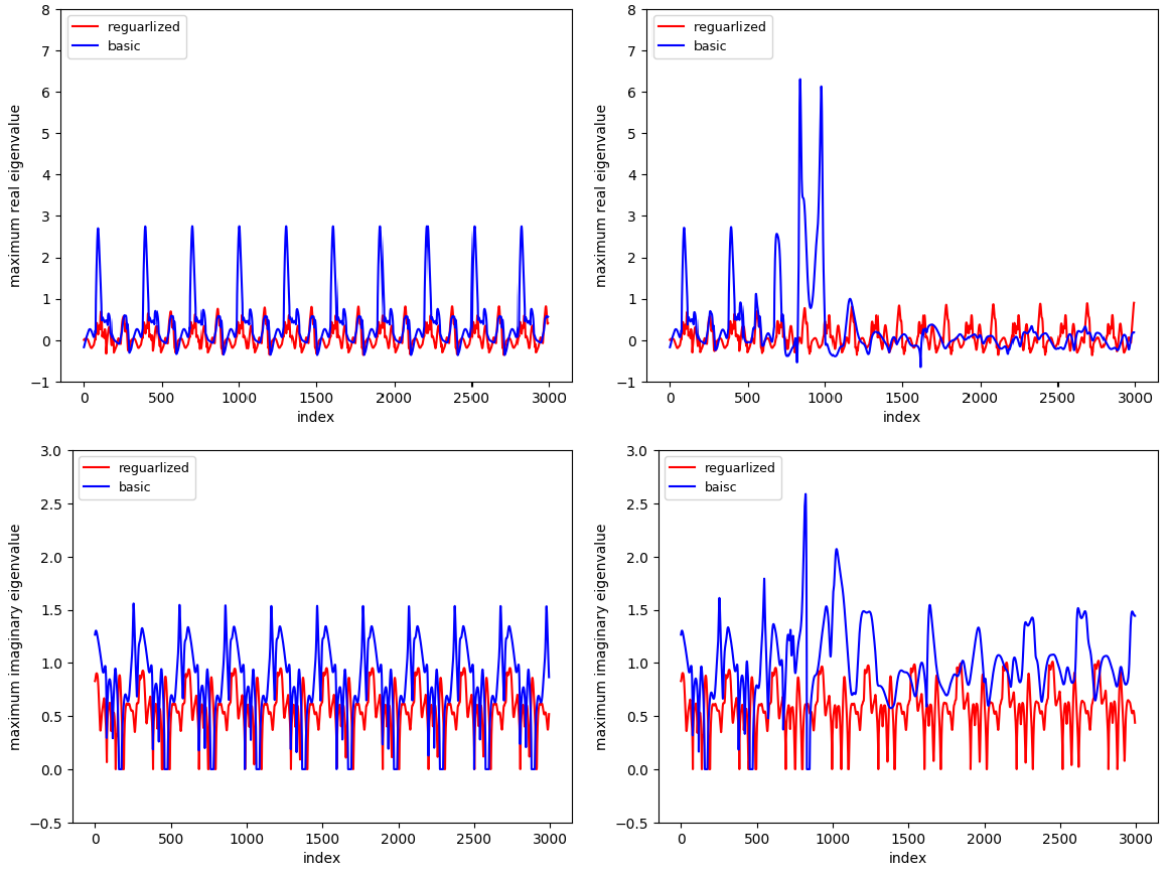


Fig. 17 Flow in cylinder wake. Comparison of eigenvalue of Jacobian between regularized and basic model on testing data. Top: maximum real eigenvalue. Bottom: maximum imaginary eigenvalue. Left: a priori. Right: a posteriori.

The Jacobian regularized model is employed with hyperparameters shown in table 4, with fig. 20 showing a posteriori evaluation on training data. The reconstruction is successful, but the performance deteriorates on testing data because the trajectory of the system does not exhibit a low dimensional attractor as in the cylinder case. Therefore the training data is not informative for predictions on the test set. For a black-box machine learning model, this phenomena can be expected to be more pronounced in high dimensional space due to data scarcity. Specifically, we discuss this problem in the following section.

Table 4 Hyperparameter configuration of Jacobian regularized model for buoyant mixing flow.

layer structure	activation function	loss function	optimizer	learning rate	λ
10-20-20-10	penalized tanh [46]	MSE	Adam	0.001	$5e-4$

4.6 Improving model predictability by data augmentation

In this section, we consider two scenarios of data augmentation: (i) augmenting the information in the data by spreading training locations randomly following a uniform distribution provided

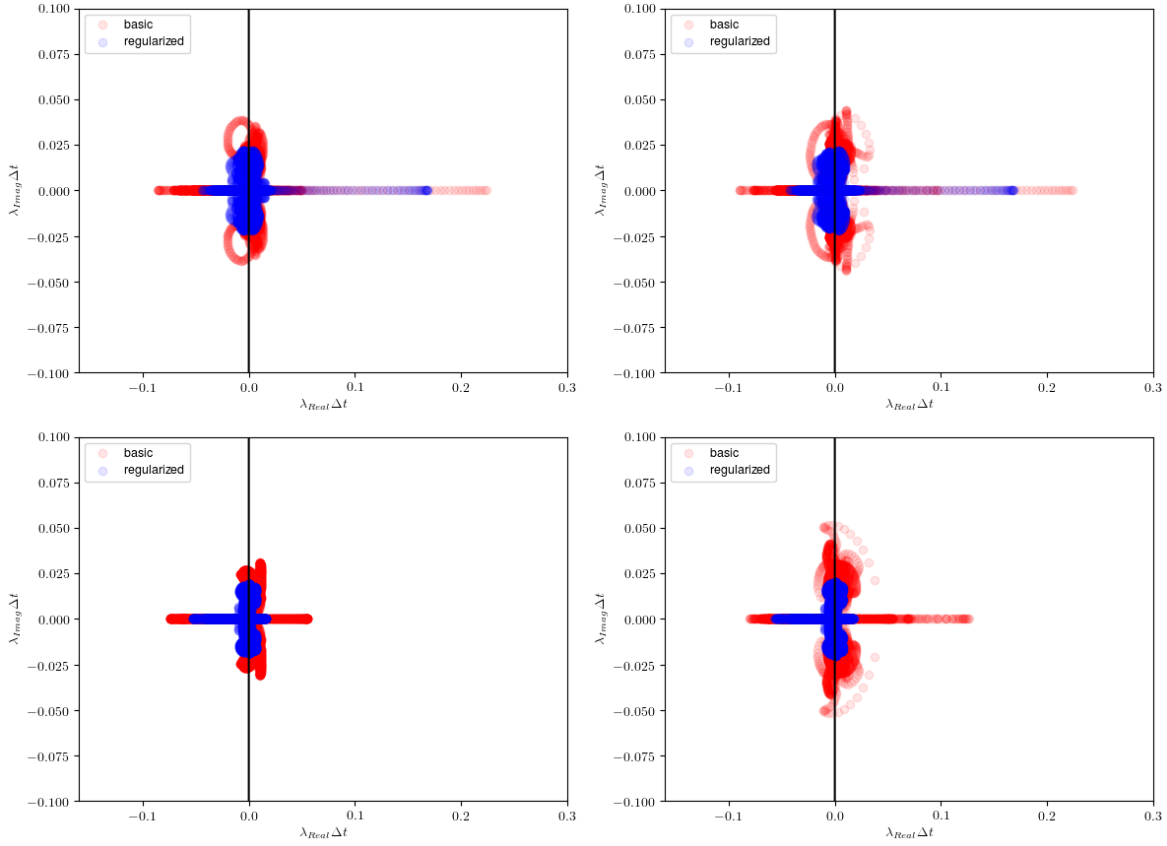


Fig. 18 Flow in cylinder wake. Comparison of linear stability diagram between regularized and basic model. Top left: a priori on training. Top right: a posteriori on training. Bottom left: a priori on testing. Bottom right: a posteriori on testing.

that one has access to true \mathbf{F} at any desired location; (ii) augmenting the data by assembling several trajectories generated from different initial conditions.

4.6.1 Random uniform sampling in phase space

Recall that, in the two-dimensional problems in section 4.1 and section 4.2, the stepwise error contour shows that local error increases on testing scenarios located far away from the training data which was highly concentrated in a compact region of phase space. Without any knowledge of system behavior, it is sensible to start with training data from a random uniform distribution in a compact region of phase space corresponding to interesting dynamics. To conduct a thorough stepwise error contour evaluation of the training target in phase space, the VDP system is chosen to illustrate this idea.

Determining the most informative data samples would potentially involve specific knowledge of the underlying system and the models used, and is beyond the scope of current work. Here we simply consider uniform random sampling in the phase space in a finite domain: $[-3, 3]$ for the first component and $[-5, 5]$ for the second component. We obtained a new set of 399 training data points using random uniform sampling in phase space while retaining the same testing data as in section 4.1.

The performance of the basic model with the same hyperparameter setting as in section 4.1 on randomly distributed training data is shown in fig. 21. While the number of data points has

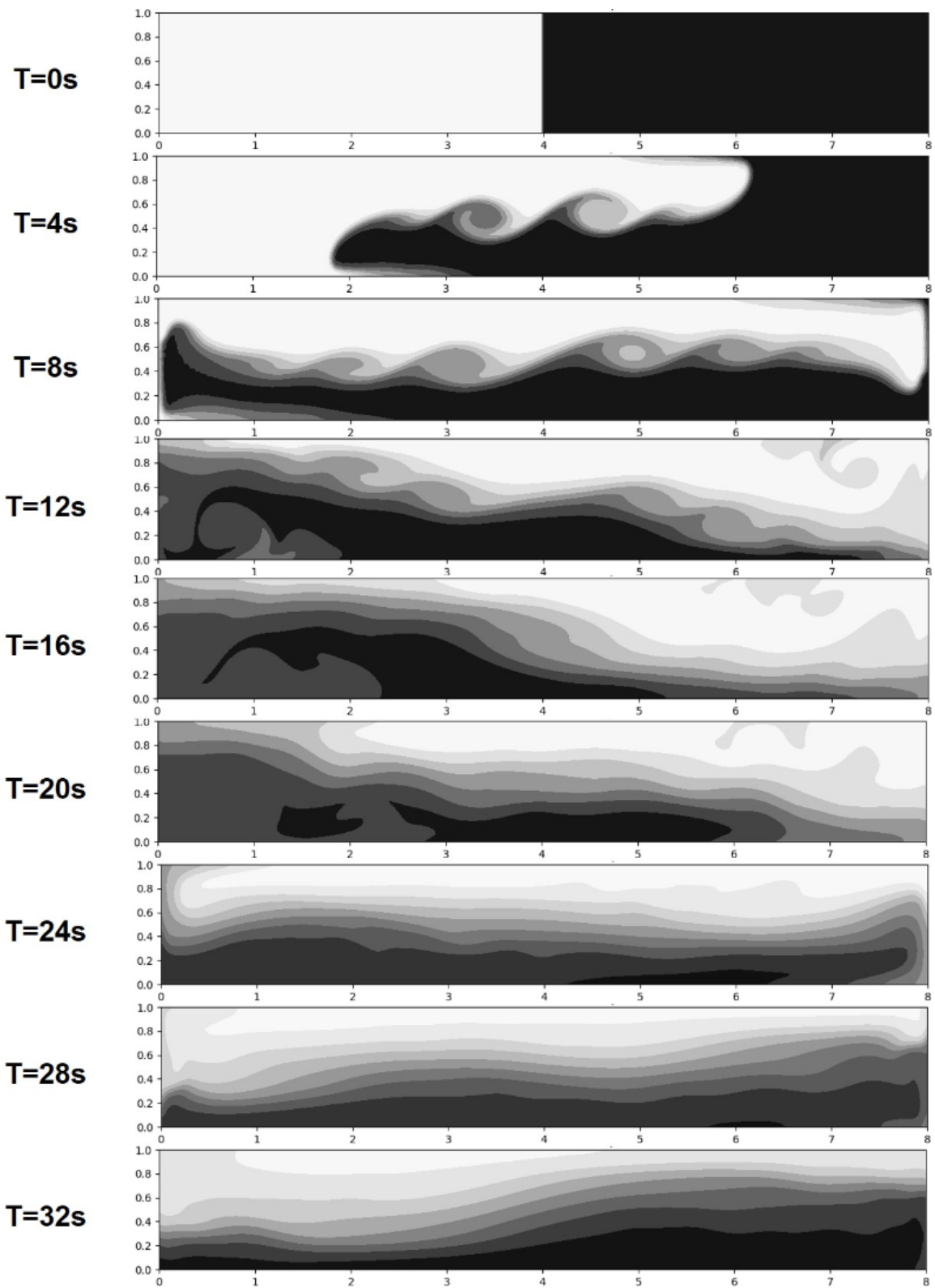


Fig. 19 Buoyant mixing flow. Time evolution of the temperature field.

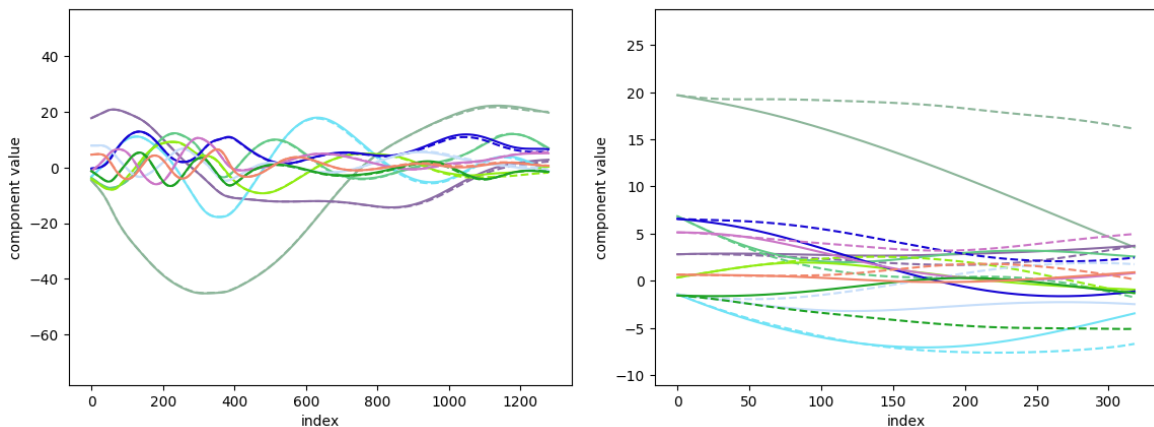


Fig. 20 A posteriori comparison between prediction of Jacobian regularized model and ground truth for POD coefficient of buoyant mixing flow. Dashed: model. Solid: ground truth. First mode: ●. Second mode: ●. Third mode: ●. Fourth mode: ●. Fifth mode: ●. Sixth mode: ●. Seventh mode: ●. Eighth mode: ●. Ninth mode: ●. Tenth mode: ●.

not been changed, the contour error of the resulting model decreased significantly compared to training with the same number of data points in a single trajectory, which indicates an improved generalizability with the same amount of training data.

4.6.2 Training with multiple trajectories with random initialization

Training data can also be augmented by multiple trajectories with different initial conditions. Here we take the one-dimensional viscous Burgers equation shown in eq. (29) as example.

The initial conditions are generated following a specific energy spectrum [47,27] shown in eq. (30).

$$\frac{\partial u}{\partial t} + u \frac{\partial u}{\partial x} = \nu \frac{\partial^2 u}{\partial x^2}, \quad (29)$$

where $x \in [0, 2\pi]$ is a periodic domain discretized using 2048 uniformly distributed grid points, and $t \in [0, 20]$, $\nu = 0.01$.

$$u(x, 0) = \sum_{k=1}^{k_c} \frac{1}{\pi} \sqrt{2AE(k)} \sin(kx + \beta_k), \quad (30)$$

where for each k , β_k is a random number drawn from a uniform distribution on $[-\pi, \pi]$, $E(k) = 5^{-5/3}$ if $1 \leq k \leq 5$, $A = 25$, and $E(k) = k^{-5/3}$ if $k > 5$. Multiple trajectories are generated using different seeds for random numbers to obtain the trajectories of the full-order system. To fully resolve the system as a DNS, eq. (29) is solved using a standard pseudo-spectral method with SSP-RK3 [48] for time stepping. Here we choose $k_c = 2$. Discrete cosine transformation (DCT) is used to reduce the dimension of the full system to first 4 cosine modes in the system where around 97% of kinetic energy is preserved. For simplicity, we seek a closed Markovian reduced-order-system, whereas the underlying dynamics is clearly non-Markovian [49,27].

Since the first component of the DCT is constant, the remaining components of feature space are shown in fig. 22. The training data is far away from the testing data initially, whereas the data converges at a later stage. This is because of the presence of a spiral fixed point attractor resulting from the viscous dissipative nature of the system. Therefore, if the model is only trained from a single trajectory, it will be very difficult for the model to generalize well in the phase space especially where the state of the system is not near an attractor.

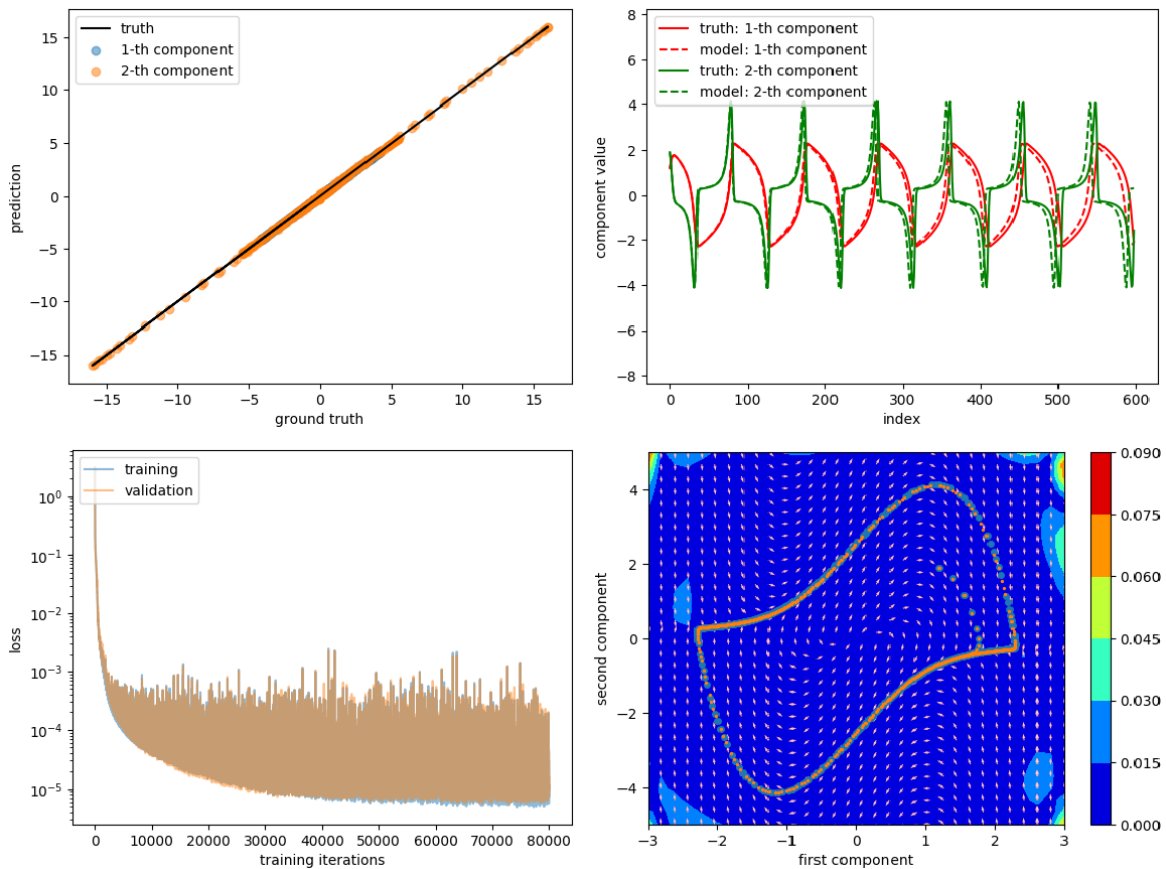


Fig. 21 A priori and a posteriori result of the basic model on the VDP system, training with random sampled data distribution. Top left: a priori evaluation. Top right: a posteriori evaluation. Bottom left: learning curve. Bottom right: stepwise error contour. Blue dot: ground truth. Orange dot: prediction. White arrow: direction of target vector of ground truth. Red arrow: direction of target vector of prediction.

Many dynamical systems in nature exhibit attractors in the asymptotic sense. From the viewpoint of data-driven modeling of such dynamics, data scarcity is encountered at the start of trajectory where the number of trajectories required to provide enough information to cover the region of interest grows exponentially. Much research on applying neural network-based models for dynamical systems [16][22][33] demonstrate problems starting on limit cycles or chaotic attractors in a low-dimensional feature space, where the issue of initial data scarcity is not significant, or can be easily alleviated by a small increase in available data. However, for the purpose of modeling phenomena such as turbulent fluid flow, which can be high dimensional even after dimension reduction, the model would likely fail for long-time prediction due to data scarcity. Such a situation may be realized in regions of phase space where the state has not arrived at the low manifold attractor. Therefore, the training data might not be representative of testing data which violates the fundamental assumption of a well-posed machine learning problem [50]. Moreover, data scarcity will shrink the region of generalizability of the model as the dimension of the system increases.

A key benefit of using a neural network model is its linear growth in complexity with dimension of the system, in contrast to traditional polynomial regression methods [34]. However, initial data scarcity would limit the generalizability of a ANN in modeling a high dimensional dynamical system that does not exhibit a low dimensional attractor. We believe this phenomenon

of data scarcity observed from this simple nonlinear PDE example also applies to other nonlinear dynamical systems.

To alleviate the initial data scarcity issue, a solution is to augment the training data with more trajectories with different random number seeds in generating the initial condition, while keeping the energy spectrum the same across all cases. In this case we choose 18 such trajectories. Each trajectory contains states of 1000 snapshots equally spaced in time. For testing data, we simply consider one DNS result with an initial condition different from all training trajectories. The corresponding training and testing trajectories are visualized in phase space as shown in fig. 22.

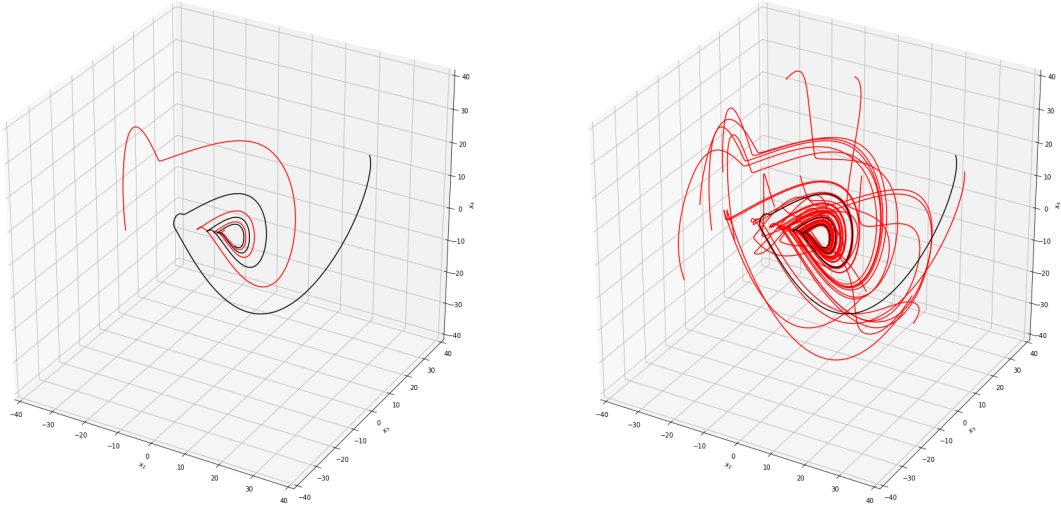


Fig. 22 Feature distribution of training/testing data for component x_2, x_3, x_4 . Left: with one training trajectory. Right: with 18 training trajectory. Black line: testing. Red line: training.

The basic model is trained with hyperparameters in table 5 and 1000 epochs. The resulting learning curve and a posteriori evaluation are shown in fig. 23. Relatively large discrepancy is observed near the initial condition as the initial data scarcity is not completely eliminated due to limited number of additional trajectories. Increasing the number of additional trajectories, may be unaffordable for very high dimensional systems. Moreover, the result also shows that the error decreases once the trajectory falls on the fixed point attractor. Thus, if the model starts in the low dimensional attractor where the information is well-preserved in the training data, better performance might be expected. This hypothesis is consistent with previous work [33], where successful prediction of future states starts at the time when the states converge to a low dimensional attractor.

Table 5 Hyperparameter configuration of basic model: VBE system with four modes

layer structure	activation function	loss function	optimizer	learning rate
4-30-30-30-4	elu	MSE	Adam	0.0005

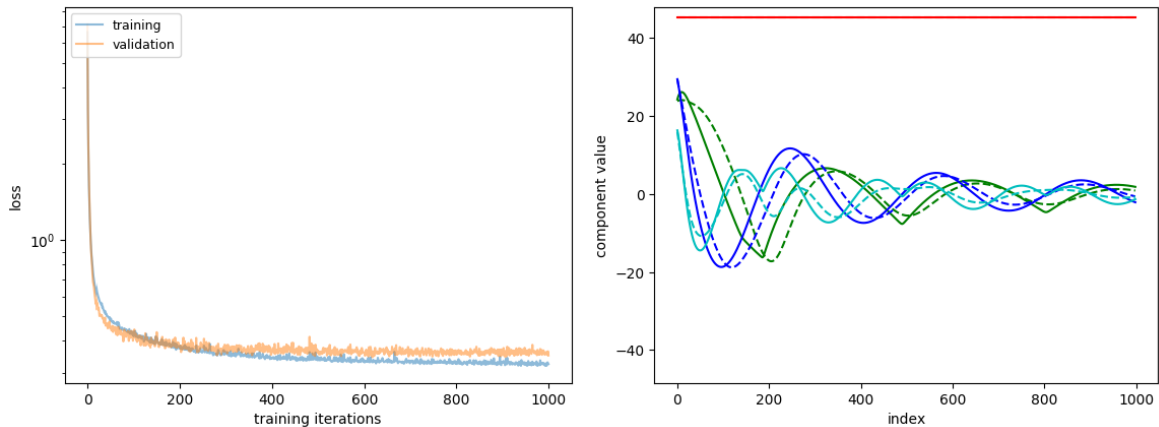


Fig. 23 Result of basic model for one dimensional VBE turbulence case. Left: learning curve. Right: a posteriori result with augmented training trajectories. Red: x_1 . Green: x_2 . Blue: x_3 . Cyan: x_4 . Dashed: model prediction. Solid: ground truth.

5 Conclusions

This work investigated the modeling of dynamical systems using feedforward neural networks (FNN), with a focus on long time prediction. It was shown that neural networks have advantages over sparse polynomial regression in terms of adaptability, but with a trade-off in training cost. From the perspective of global error analysis and the observation of the strong correlation between the local error and maximum singular value of the Jacobian, we propose the suppression of the Frobenius norm of the Jacobian as regularization. This showed promise in improving the robustness of the basic FNN model given limited data, or when the model has a non-ideal architecture, or when the model is unstable. The effectiveness of Jacobian regularization is attributed to finding a balance between lowering the prediction error, and suppressing the sensitivity of the prediction of the future state to the current local error. In terms of modeling dynamical systems that do not involve low-dimensional attractors, limitations of FNNs, and perhaps all local ML methods, was demonstrated in a buoyant mixing flow. Challenges were noted in the example of the reduced-order viscous burgers system, where significant initial data scarcity is present. Augmenting the data either by altering the distribution of training data in phase space or by simply adding multiple trajectories from different initial conditions resulted in improvement of the performance of FNN model to some extent. However, these remedies require a significant amount of additional sampling in phase space, especially for high dimensional system which suffers from the curse of dimensionality.

Acknowledgements The authors gratefully acknowledge Zejia Zhang for polishing the paper and Professor Balaji Jayaraman for helpful discussion, comments and providing the POD data of two dimensional instability-driven buoyant mixing flows. This work is financially supported by Air Force Office of Scientific Research grant: "Modeling of Non-local Effects using Statistical Coarse-graining".

References

1. M. Tanaskovic, L. Fagiano, C. Novara, M. Morari, *Automatica* **75**, 1 (2017)
2. R.H. Shumway, D.S. Stoffer, *Studies In Informatics And Control* **9**(4), 375 (2000)
3. S.L. Brunton, J.L. Proctor, J.N. Kutz, *arXiv* **1**(609), 1 (2015). DOI 10.1073/pnas.1517384113. URL <http://arxiv.org/abs/1509.03580>

4. N.M. Mangan, S.L. Brunton, J.L. Proctor, J.N. Kutz, IEEE TRANSACTIONS ON MOLECULAR, BIOLOGICAL, AND MULTI-SCALE COMMUNICATIONS **2**(1), 52 (2017). DOI 10.1109/TMBMC.2016.2633265
5. O. Russakovsky, J. Deng, H. Su, J. Krause, S. Satheesh, S. Ma, Z. Huang, A. Karpathy, A. Khosla, M. Bernstein, et al., International Journal of Computer Vision **115**(3), 211 (2015)
6. A. Karpathy, G. Toderici, S. Shetty, T. Leung, R. Sukthankar, L. Fei-Fei, in *Proceedings of the IEEE conference on Computer Vision and Pattern Recognition* (2014), pp. 1725–1732
7. T. Duriez, S.L. Brunton, B.R. Noack, *Machine Learning Control-Taming Nonlinear Dynamics and Turbulence* (Springer, 2017)
8. K. Hornik, Neural networks **4**(2), 251 (1991)
9. K.S. Narendra, K. Parthasarathy, IEEE transactions on neural networks / a publication of the IEEE Neural Networks Council **1**(1), 4 (1990). DOI 10.1109/72.80202
10. M. Polycarpou, P. Ioannou, University of Southern California (September) (1991)
11. K.S. Narendra, K. Parthasarathy, International Journal of Approximate Reasoning **6**(2), 109 (1992). DOI 10.1016/0888-613X(92)90014-Q
12. J.G. Kuschewski, S.H. Žak, S. Hui, IEEE Transactions on Control Systems Technology **1**(1), 37 (1993). DOI 10.1109/87.221350
13. S.A. Billings, H.B. JAMALUDDIN, S. Chen, International Journal of Control **55**(1), 193 (1992). DOI 10.1080/00207179208934232. URL <http://www.tandfonline.com/doi/abs/10.1080/00207179208934232>
14. V. Elanayar, Y. Shin, Neural Networks, IEEE Transactions **5**(4), 594 (1994). URL http://ieeexplore.ieee.org/xpls/abs_all.jsp?arnumber=298229
15. K. Chakraborty, K. Mehrotra, C.K. Mohan, S. Ranka, Neural Networks **5**(6), 961 (1992). DOI 10.1016/S0893-6080(05)80092-9. URL <http://www.scopus.com/scopus/inward/record.url?eid=2-s2.0-0026954346&partnerID=40>
16. F.S. Tsung, G.W. Cottrell, in *Advances in Neural Information Processing Systems* (1995), pp. 481–488
17. T.L. Paez, N. Hunter, Dynamical system modeling via signal reduction and neural network simulation. Tech. rep., Sandia National Labs., Albuquerque, NM (United States) (1997)
18. A. Urbina, N.F. Hunter, T.L. Paez, Characterization of nonlinear dynamic systems using artificial neural networks. Tech. rep., Sandia National Labs., Albuquerque, NM (United States) (1998)
19. T.L. Paez, N.F. Hunter, Nonlinear system modeling based on experimental data. Tech. rep., Sandia National Labs., Albuquerque, NM (US); Sandia National Labs., Livermore, CA (US) (2000)
20. N. Smaoui, SIAM Journal on Scientific Computing **23**(3), 824 (2001). DOI 10.1137/S1064827599355013
21. N. Smaoui, S. Al-enezi, Journal of Computational and Applied Mathematics **170**(1), 27 (2004). DOI 10.1016/j.cam.2003.12.045
22. N. Smaoui, Applied Mathematical Modelling **21**(12), 739 (1997). DOI 10.1016/S0307-904X(97)00092-9. URL <http://linkinghub.elsevier.com/retrieve/pii/S0307904X97000929>
23. J.L. Elman, Cognitive science **14**(2), 179 (1990)
24. R. Bakker, J.C. Schouten, C.L. Giles, F.C. Takens, C.M. Van Den Bleek, Neural Comput. **12**(10), 2355 (2000). DOI 10.1162/089976600300014971. URL <http://dx.doi.org/10.1162/089976600300014971>
25. H. Lin, W. Chen, A. Tsutsumi, Chemical Engineering and Processing: Process Intensification **42**(8-9), 611 (2003). DOI 10.1016/S0255-2701(02)00210-6. URL <http://www.sciencedirect.com/science/article/pii/S0255270102002106>
26. A.J. Chorin, O.H. Hald, *Stochastic tools in mathematics and science*, vol. 3 (Springer, 2009)
27. E. Parish, K. Duraisamy, 46th AIAA Fluid Dynamics Conference (June), 1 (2016). DOI 10.2514/6.2016-3640. URL <http://arc.aiaa.org/doi/10.2514/6.2016-3640>
28. T. Koskela, M. Lehtokangas, J. Saarinen, K. Kaski, In Proceedings of the World Congress on Neural Networks pp. 491–496 (1996)
29. D.S. Broomhead, G.P. King, Physica D: Nonlinear Phenomena **20**(2-3), 217 (1986)
30. T. Miyoshi, H. Ichihashi, S. Okamoto, T. Hayakawa, in *Neural Networks, 1995. Proceedings., IEEE International Conference on*, vol. 1 (IEEE, 1995), vol. 1, pp. 588–593
31. Y. Sato, S. Nagaya, in *Evolutionary Computation, 1996., Proceedings of IEEE International Conference on* (IEEE, 1996), pp. 144–149
32. C.A. Bailer-Jones, D.J. MacKay, P.J. Withers, network: computation in neural systems **9**(4), 531 (1998)
33. Z. Wang, D. Xiao, F. Fang, R. Govindan, C.C. Pain, Y. Guo, International Journal for Numerical Methods in Fluids (July), 1 (2017). DOI 10.1002/flid.4416. URL <http://doi.wiley.com/10.1002/flid.4416>
34. I. Goodfellow, Y. Bengio, A. Courville, *Deep learning* (MIT press, 2016)
35. D.E. Rumelhart, G.E. Hinton, R.J. Williams, Learning internal representations by error propagation. Tech. rep., California Univ San Diego La Jolla Inst for Cognitive Science (1985)
36. N.M. Mangan, S.L. Brunton, J.L. Proctor, J.N. Kutz, IEEE Transactions on Molecular, Biological and Multi-Scale Communications **2**(1), 52 (2016)
37. A.P. Trischler, G.M. DEleuterio, Neural Networks **80**, 67 (2016)
38. K. Hornik, M. Stinchcombe, H. White, Neural networks **2**(5), 359 (1989)

39. D. Kingma, J. Ba, arXiv preprint arXiv:1412.6980 (2014)
40. M. Abadi, A. Agarwal, P. Barham, E. Brevdo, Z. Chen, C. Citro, G.S. Corrado, A. Davis, J. Dean, M. Devin, S. Ghemawat, I.J. Goodfellow, A. Harp, G. Irving, M. Isard, Y. Jia, R. Józefowicz, L. Kaiser, M. Kudlur, J. Levenberg, D. Mané, R. Monga, S. Moore, D.G. Murray, C. Olah, M. Schuster, J. Shlens, B. Steiner, I. Sutskever, K. Talwar, P.A. Tucker, V. Vanhoucke, V. Vasudevan, F.B. Viégas, O. Vinyals, P. Warden, M. Wattenberg, M. Wicke, Y. Yu, X. Zheng, CoRR **abs/1603.04467** (2016). URL <http://arxiv.org/abs/1603.04467>
41. S. Rifai, X. Glorot, Y. Bengio, P. Vincent, arXiv preprint arXiv:1104.3250 (2011)
- 42.
43. E. Weinan, C.W. Shu, *Phys.Fluids* **6(1)** (1994). DOI 10.1063/1.868044
44. W.C. Liu, J.-G., H. Johnston, *J. Sci. Comp* **18(2)** (2003). DOI 10.1002/fld.4006
45. O. San, J. Borggaard, *Int. J. Num. Meth. Engg.* **78** (2015). DOI 10.1002/fld.4006
46. B. Xu, R. Huang, M. Li, arXiv preprint arXiv:1602.05980 (2016)
47. Y. Li, Z. Wang, *Computers & Fluids* **139**, 92 (2016)
48. S. Gottlieb, C.W. Shu, E. Tadmor, *SIAM review* **43(1)**, 89 (2001)
49. S. Pan, K. Duraisamy, arXiv preprint arXiv:1803.09318 (2018)
50. J. Friedman, T. Hastie, R. Tibshirani, *The elements of statistical learning*, vol. 1 (Springer series in statistics New York, 2001)